Cuerpos Menores

Material complementario del curso Planetología 2014

Tabaré Gallardo

www.astronomia.edu.uy/depto/planetologia/planet.html

Table 11.1 **Half-Lives of Selected Nuclides**

Parent	Measurable Stable Daughter(s)	Half-Life ($t_{1/2}$)
Long-lived radionuclides		
^{40}K	^{40}Ar, ^{40}Ca	1.25 Gyr
^{87}Rb	^{87}Sr	48 Gyr
^{147}Sm	^{143}Nd, ^{4}He	106 Gyr
^{187}Re	^{187}Os	44 Gyr
^{232}Th	^{208}Pb, ^{4}He	14 Gyr
^{235}U	^{207}Pb, ^{4}He	0.704 Gyr
^{238}U	^{206}Pb, ^{4}He	4.47 Gyr
Extinct radionuclides		
^{10}Be	^{10}B	1.4 Myr
^{22}Na	^{22}Ne	2.6 yr
^{26}Al	^{26}Mg	0.72 Myr
^{36}Cl	^{36}Ar, ^{36}S	0.30 Myr
^{41}Ca	^{41}K	0.10 Myr
^{44}Ti	^{44}Sc	52 yr
^{53}Mn	^{53}Cr	3.6 Myr
^{60}Fe	^{60}Ni	2.4 Myr
^{92}Nb	^{92}Zr	35 Myr
^{99}Tc	^{99}Ru	0.21 Myr
^{107}Pd	^{107}Ag	6.5 Myr
^{129}I	^{129}Xe	16 Myr
^{146}Sm	^{142}Nd	68 Myr
^{182}Hf	^{182}W	9 Myr
^{244}Pu	$^{131-136}$Xe	82 Myr

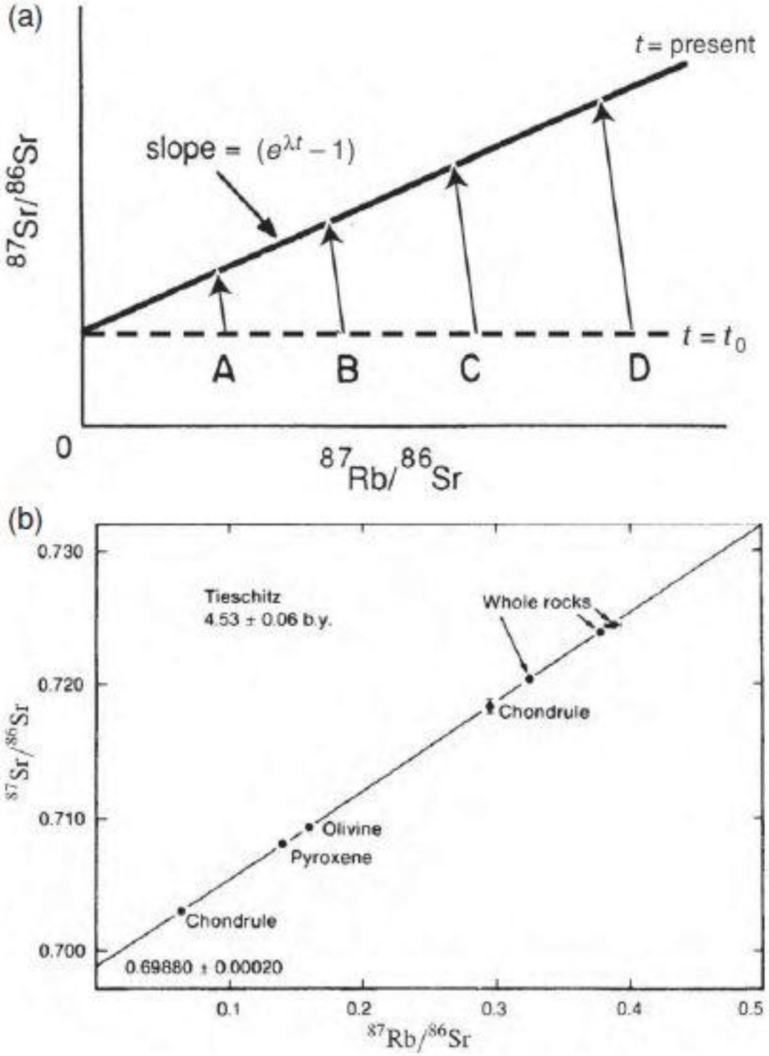

Figure 11.18 (a) Schematic isochron diagram of the ^{87}Rb–^{87}Sr system. Phases A, B, C and D have identical initial ^{87}Sr/^{86}Sr ratios at $t = 0$, but differing ^{87}Rb/^{86}Sr ratios. Assuming that the system remains closed, these ratios evolve as shown by the arrows to define an isochron for which t is the age of the rock. (de Pater and Lissauer, 2010) (b) ^{87}Rb–^{87}Sr isochron for the Tieschitz unequilibrated H3 chondrite meteorite. (Taylor 1992)

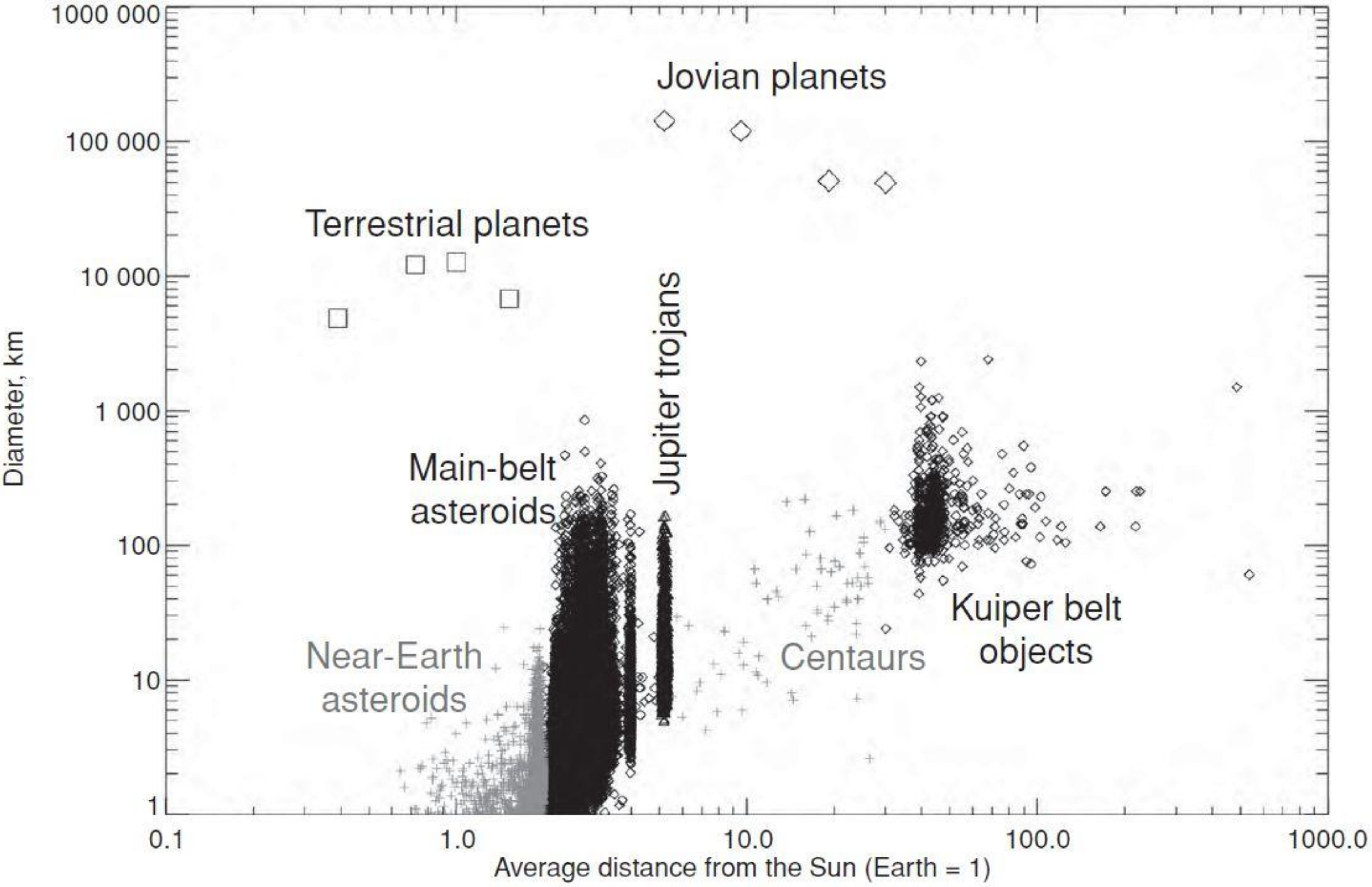
Jovian planets
Terrestrial planets
Jupiter trojans
Main-belt asteroids
Kuiper belt objects
Centaurs
Near-Earth asteroids
Diameter, km
1000 000
100 000
10 000
1 000
100
10
1
0.1
1.0
10.0
100.0
1000.0
Average distance from the Sun (Earth = 1)

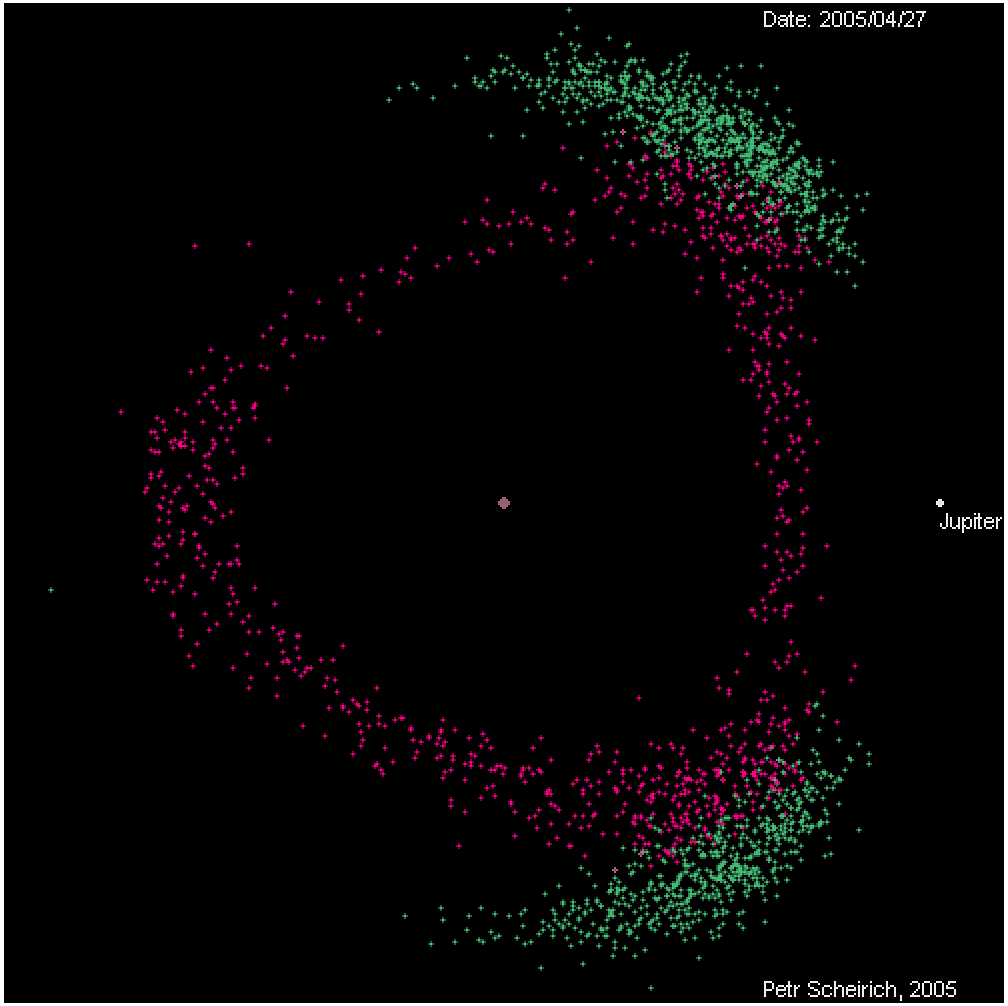
Date: 2005/04/27
Jupiter
Petr Scheirich, 2005

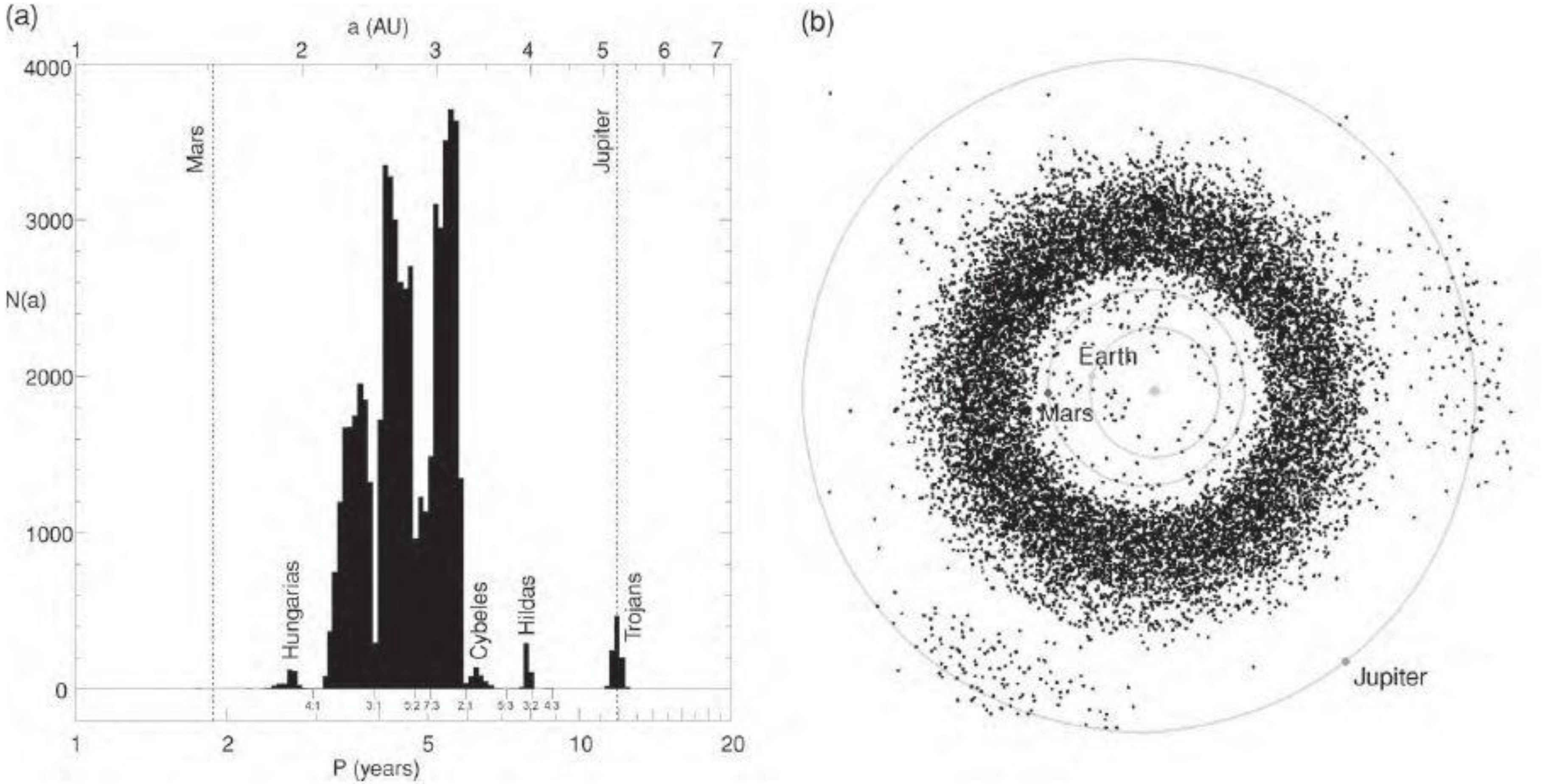

Figure 12.2 (a) Histogram of asteroids versus orbital period (with corresponding semimajor axes shown on the upper scale); the scale of the abscissa is logarithmic. All of the asteroids represented have $M_v < 15$; the 100 000 such asteroids with the smallest numbers are included. The planets Mars and Jupiter are shown by *dashed vertical lines*. Note the prominent gaps in the distribution for orbital periods 1/4, 1/2, 2/5, 3/7 and 1/3 that of Jupiter. One asteroid, Thule, is located at the 4:3 resonance. (Courtesy A. Dobrovolskis) (b) Locations projected onto the ecliptic plane of approximately 7000 asteroids on 7 March 1997. The orbits and locations of the Earth, Mars and Jupiter are indicated, and the Sun is represented by the dot in the center. (Courtesy Minor Planet Center)

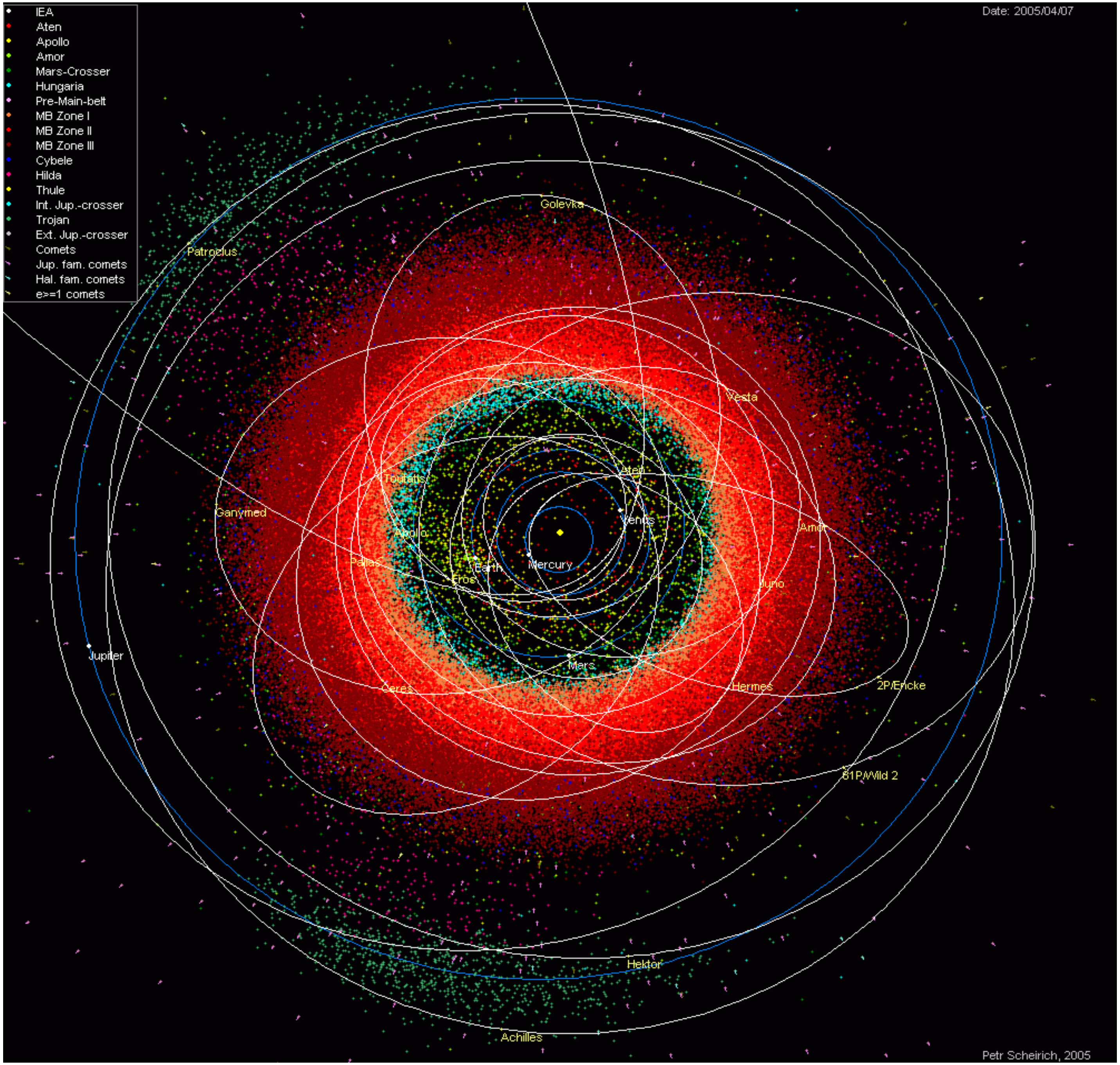
IEA
Aten
Apollo
Amor
Mars-Crosser
Hungaria
Pre-Main-belt
MB Zone I
MB Zone II
MB Zone III
Cybele
Hilda
Thule
Int. Jup.-crosser
Trojan
Ext. Jup.-crosser
Comets
Jup. fam. comets
Hal. fam. comets
e>=1 comets
Date: 2005/04/07
Golevka
Patroclus
Vesta
Toutatis
Aten
Ganymed
Venus
Amor
Apollo
Mercury
Pallas
Earth
Eros
Juno
Jupiter
Mars
Ceres
Hermes
2P/Encke
81P/Wild 2
Hektor
Achilles
Petr Scheirich, 2005

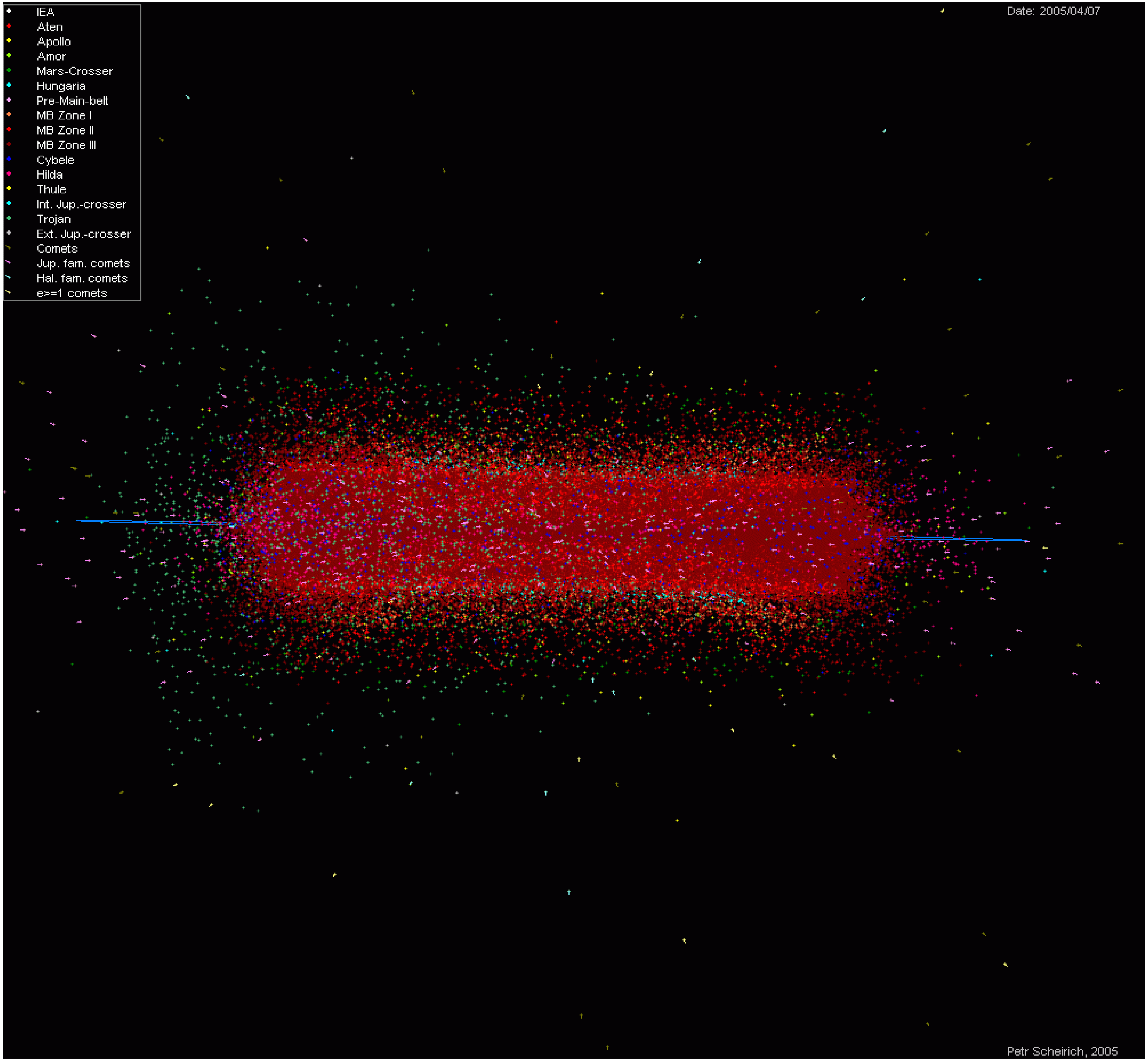
IEA
Aten
Apollo
Amor
Mars-Crosser
Hungaria
Pre-Main-belt
MB Zone I
MB Zone II
MB Zone III
Cybele
Hilda
Thule
Int. Jup.-crosser
Trojan
Ext. Jup.-crosser
Comets
Jup. fam. comets
Hal. fam. comets
e>=1 comets
Date: 2005/04/07
Petr Scheirich, 2005

Table E.6 **Eight Largest Asteroids ($a < 6$ AU)**

#	Name	Tax. Class	M_v	Radius[a] (km)	A_0	a (AU)	e	i (deg)	P_{orb} (yr)	P_{rot} (hr)	Axial Tilt (deg)
1	Ceres	C/G	3.34	467.6	0.09	2.766	0.080	10.59	4.607	9.075	9
4	Vesta	V	3.20	264.5	0.42	2.362	0.090	7.13	3.629	5.342	32
2	Pallas	B	4.13	256	0.16	2.772	0.231	34.88	4.611	7.811	110
10	Hygiea	C	5.43	203.6	0.07	3.137	0.118	3.84	5.56	27.623	126
511	Davida	C	6.22	163	0.05	3.166	0.186	15.94	5.63	5.130	65
704	Interamnia	F	5.94	158.3	0.07	3.062	0.150	17.29	5.36	8.727	60
52	Europa	C	6.31	151.3	0.06	3.099	0.104	7.48	5.460	5.631	52
87	Sylvia	P/X	6.94	143.0	0.04	3.489	0.080	10.86	6.52	5.184	35

All orbital data are from http://ssd.jpl.nasa.gov/.

[a] Mean radius; most asteroids are substantially nonspherical.

Table E.8 Masses, Radii and Densities of Selected Minor Planets

Body	Class[a]	Mass (10^{19} kg)	R (km)	ρ (kg m^{-3})	Method
Near-Earth Asteroids					
433 Eros	S	$6.7 \pm 0.3 \times 10^{-4}$	18.7	2670 ± 30	Orbiting spacecraft
25143 Itokawa	S	$3.5 \pm 0.1 \times 10^{-9}$	0.18 ± 0.01	1900 ± 130	Orbiting spacecraft
Main Belt Asteroids					
1 Ceres	C	94.3 ± 0.7	467.6 ± 2.2	2210 ± 40	Orbit perturbation
2 Pallas	C	23.9 ± 0.6	256 ± 3	3400 ± 900	Orbit perturbation
4 Vesta	V	26.7 ± 0.3	264.5 ± 5	3440 ± 120	Orbit perturbation
10 Hygiea	C	10 ± 4	203.6 ± 3.4	2760 ± 1200	Orbit perturbation
87 Sylvia	P	1.48 ± 0.01	143	1200 ± 100	Multiple system
90 Antiope	C	0.083 ± 0.002	42.9 ± 0.5	1250 ± 50	Binary system
216 Kleopatra	M	0.464 ± 0.002	67.5 ± 1	3600 ± 200	Multiple system
243 Ida	S	0.0042 ± 0.0006	15.7	2600 ± 500	Spacecraft encounter
253 Mathilde	C	0.0103 ± 0.0004	26.5	1300 ± 200	Spacecraft encounter
Trojan Asteroids					
617 Patroclus	P	0.136 ± 0.011	61 × 56	800 ± 200	Binary system
624 Hektor	D	1.0 ± 0.1	190×100×100	1600 ± 300	Binary system
Trans-Neptunian Objects					
20000 Varuna	CKBO		355^{+80}_{-65}	990^{+90}_{-20}	Shape equilibrium
134340 Pluto	RKBO	1305 ± 62	1153 ± 10	2030 ± 600	Multiple system
Charon	Moon	152 ± 6.5	606.0 ± 1.5	1650 ± 60	Multiple system
136108 Haumea	SDO	421 ± 10	725	2900 ±400	Multiple system
136199 Eris	SDO	1670 ± 20	1163 ± 6	2520 ± 50	Binary system
50000 Quaoar	CKBO	160 ± 30	445 ± 35	4200±1300	Binary system

Most data from Table 9.5 of de Pater and Lissauer (2010).

CKBO, classical Kuiper belt object; RKBO, resonant Kuiper belt object; SDO, scattered disk object.

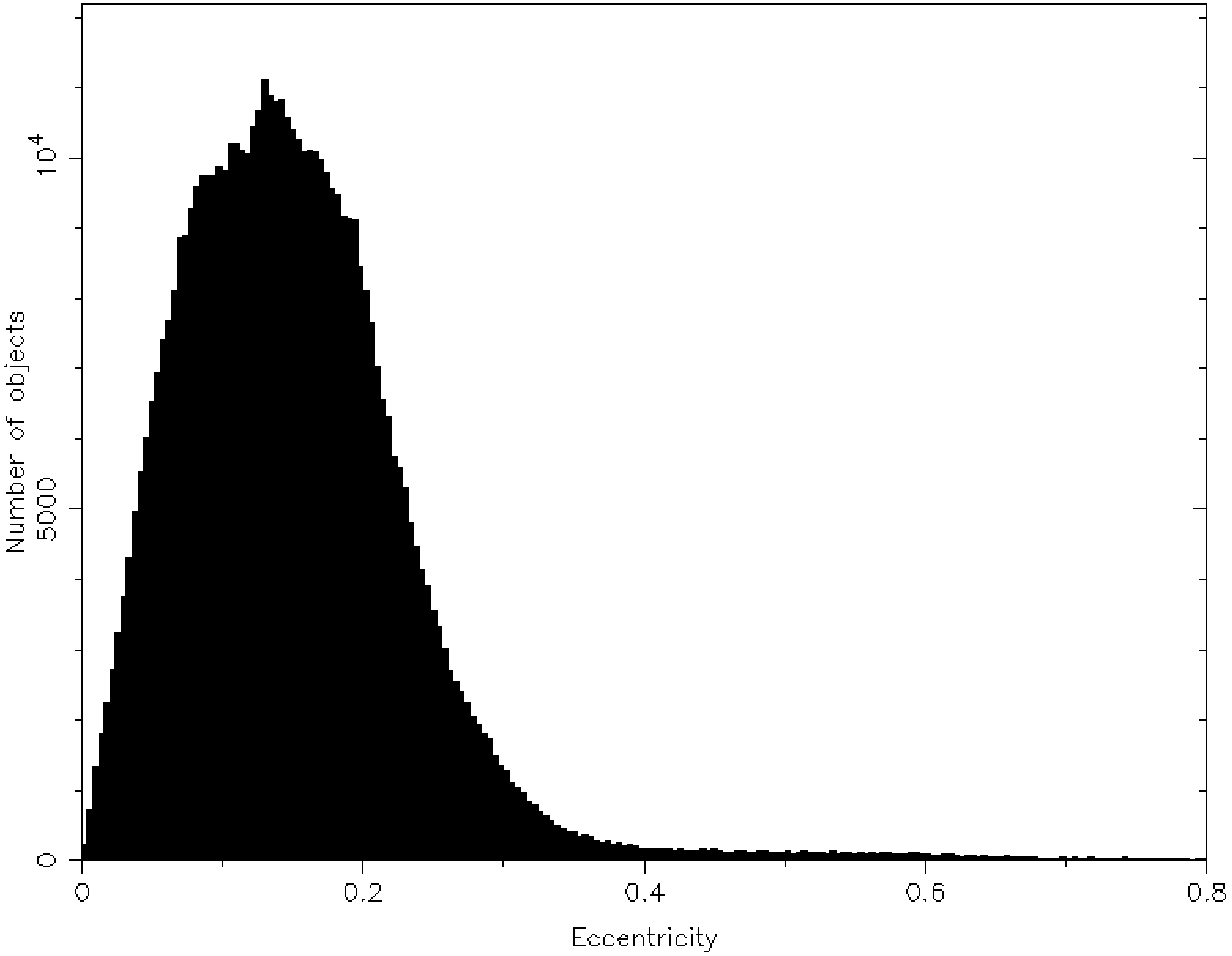

Distribution of the Minor Planets: Eccentricity

Prepared 2014 Mar. 20. (C) 2014 Minor Planet Center.

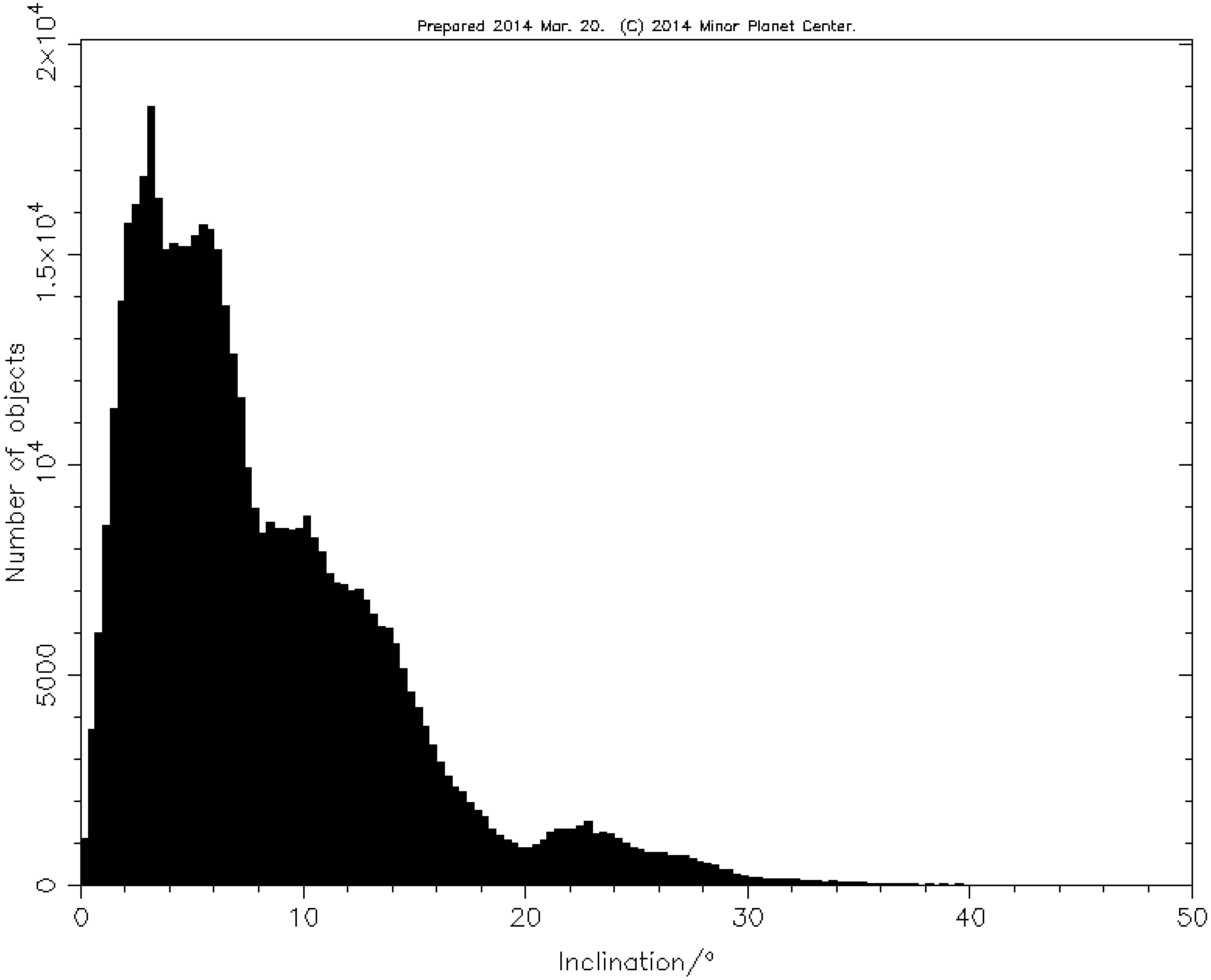

Distribution of the Minor Planets: Inclination

Prepared 2014 Mar. 20. (C) 2014 Minor Planet Center.

Distribution of the Minor Planets: Longitude of Perihelion

Prepared 2014 Mar. 20. (C) 2014 Minor Planet Center.

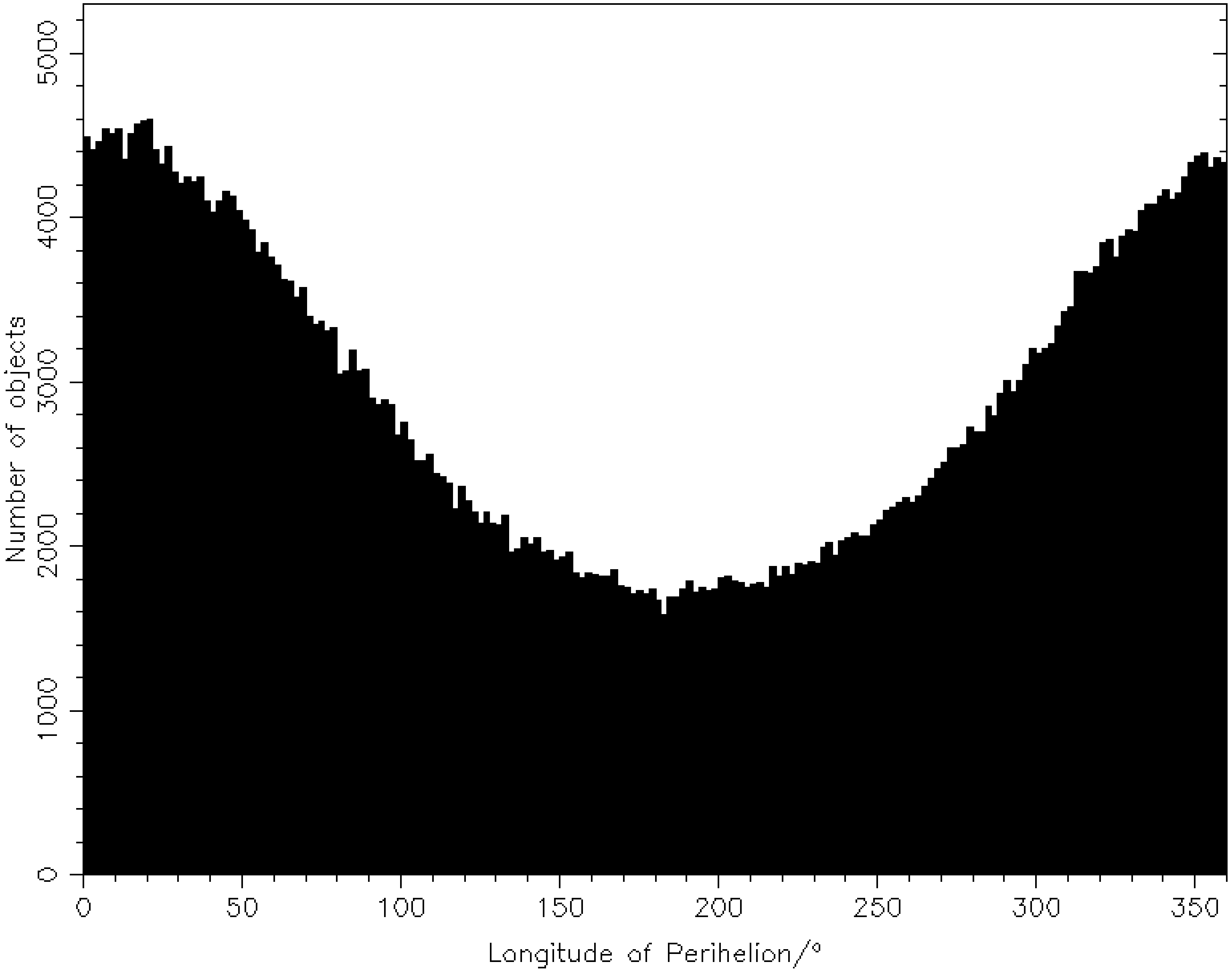

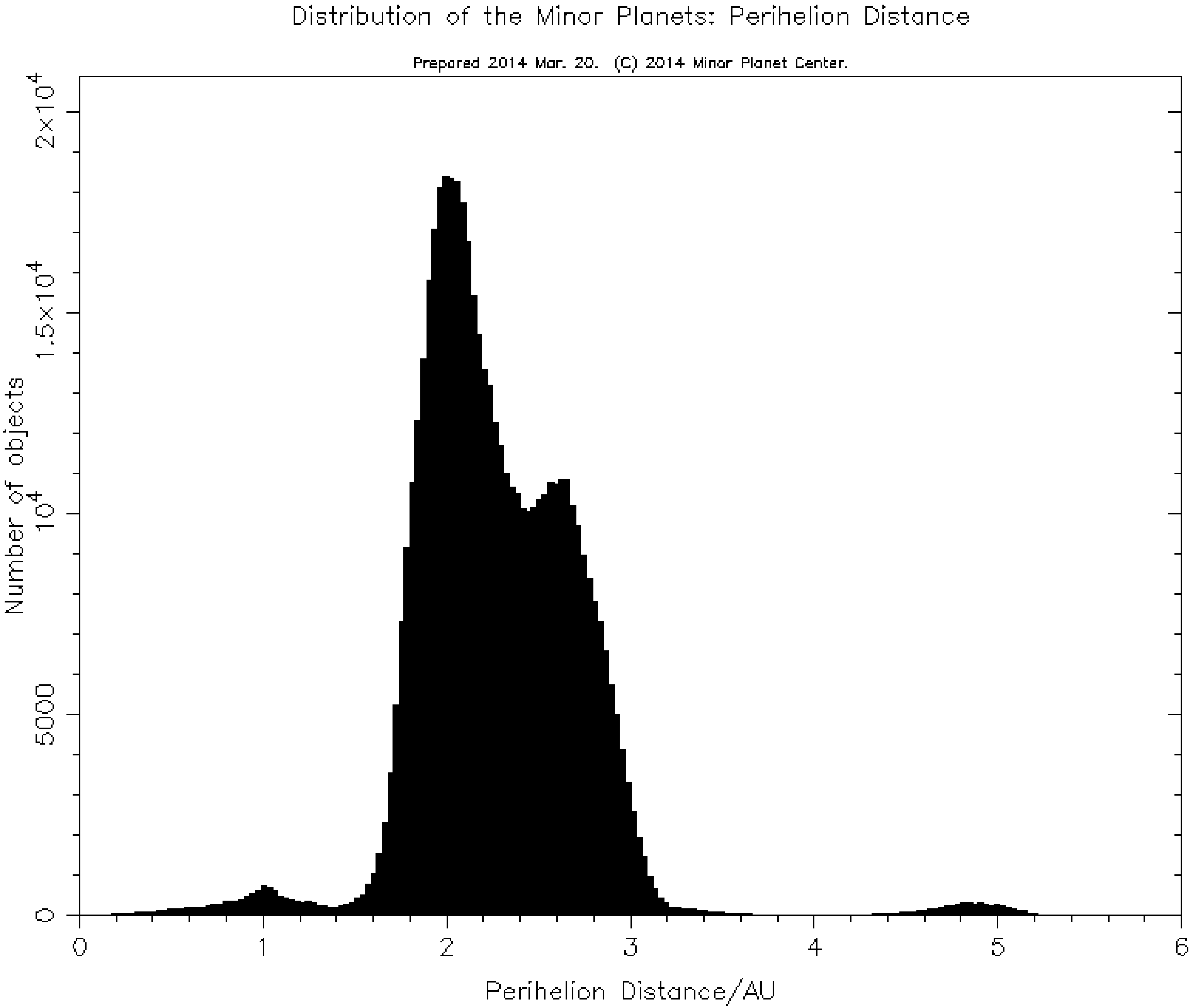
Distribution of the Minor Planets: Perihelion Distance
Prepared 2014 Mar. 20. (C) 2014 Minor Planet Center.
Number of objects
0
5000
10^4
1.5×10^4
2×10^4
0
1
2
3
4
5
6
Perihelion Distance/AU

Distribution of the Minor Planets: Absolute Magnitude

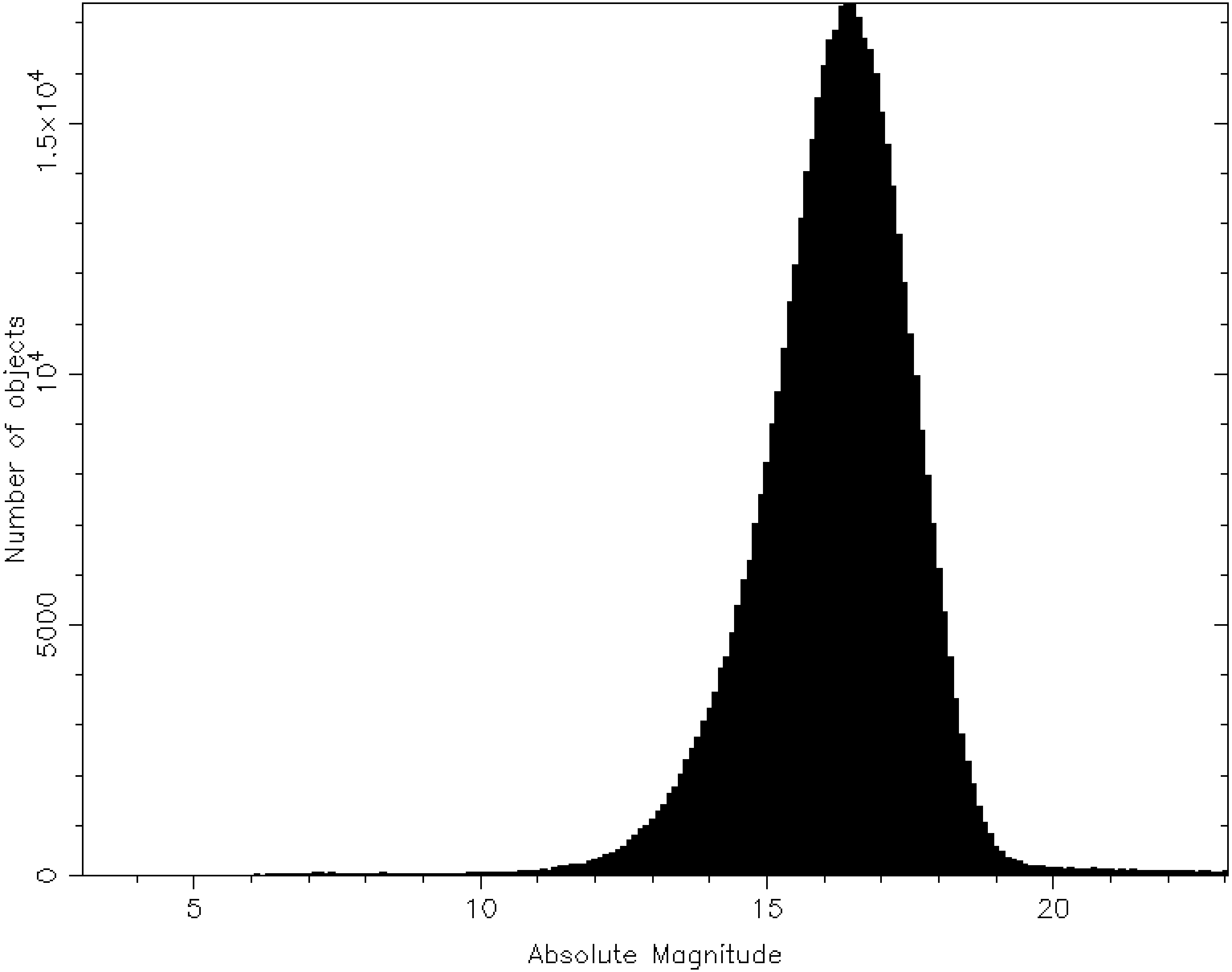

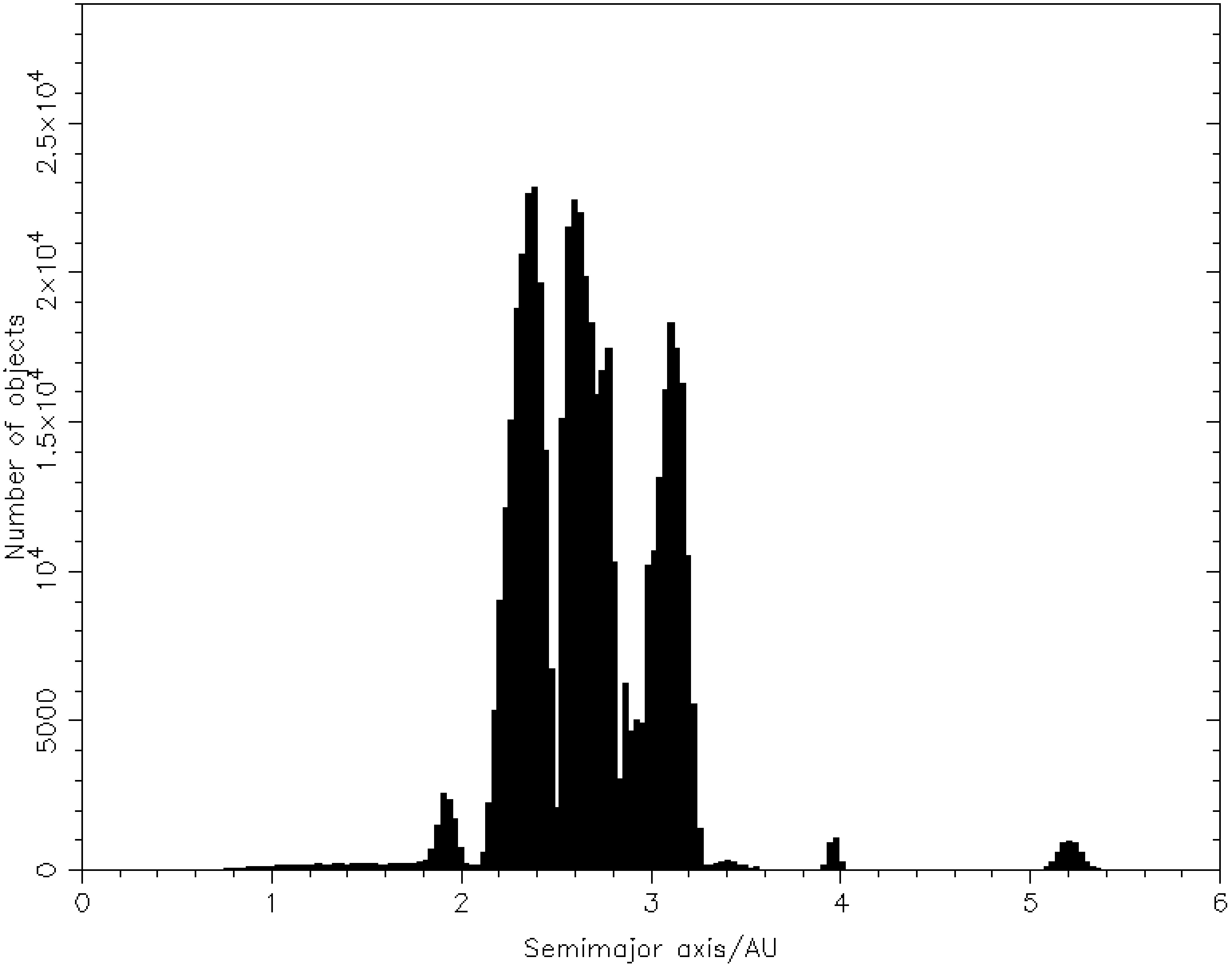

Distribution of the Minor Planets: Semimajor axis

Prepared 2014 Mar. 20. (C) 2014 Minor Planet Center.

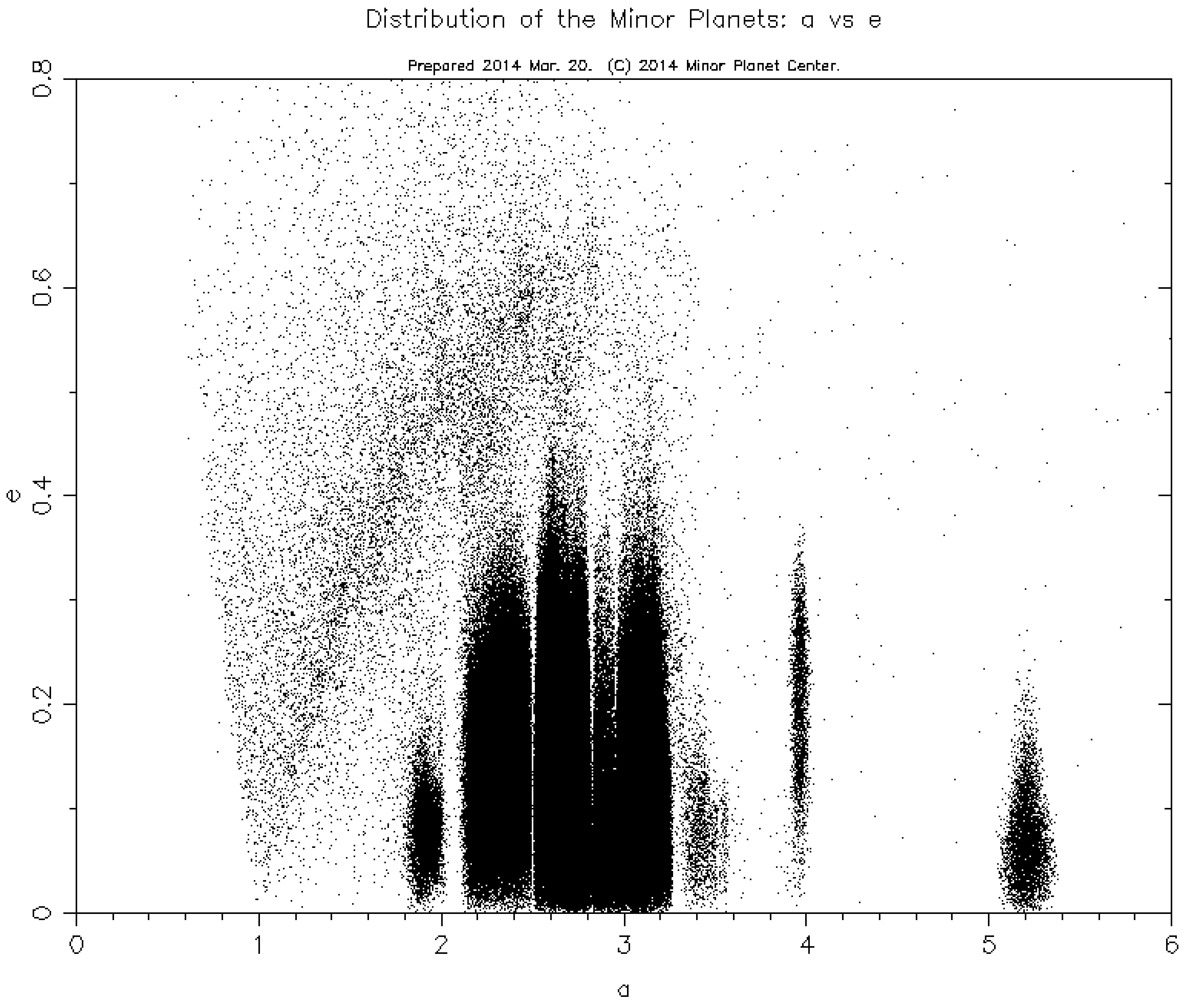

Distribution of the Minor Planets: a vs e

Prepared 2014 Mar. 20. (C) 2014 Minor Planet Center.

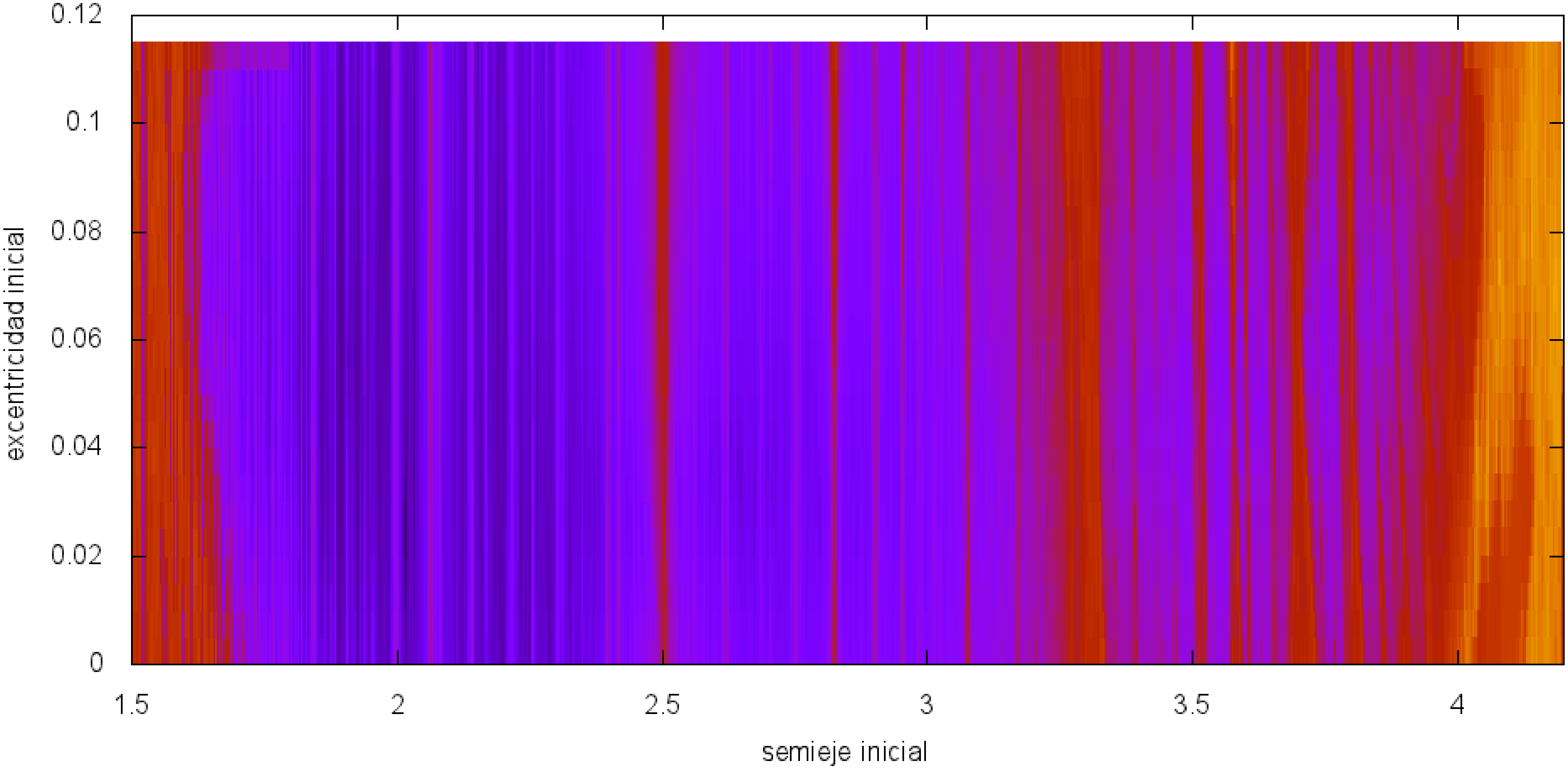
0.12
0.1
0.08
0.06
0.04
0.02
0
excentricidad inicial
1.5
2
2.5
3
3.5
4
semieje inicial

Distribution of the Minor Planets: a vs i

Prepared 2014 Mar. 20. (C) 2014 Minor Planet Center.

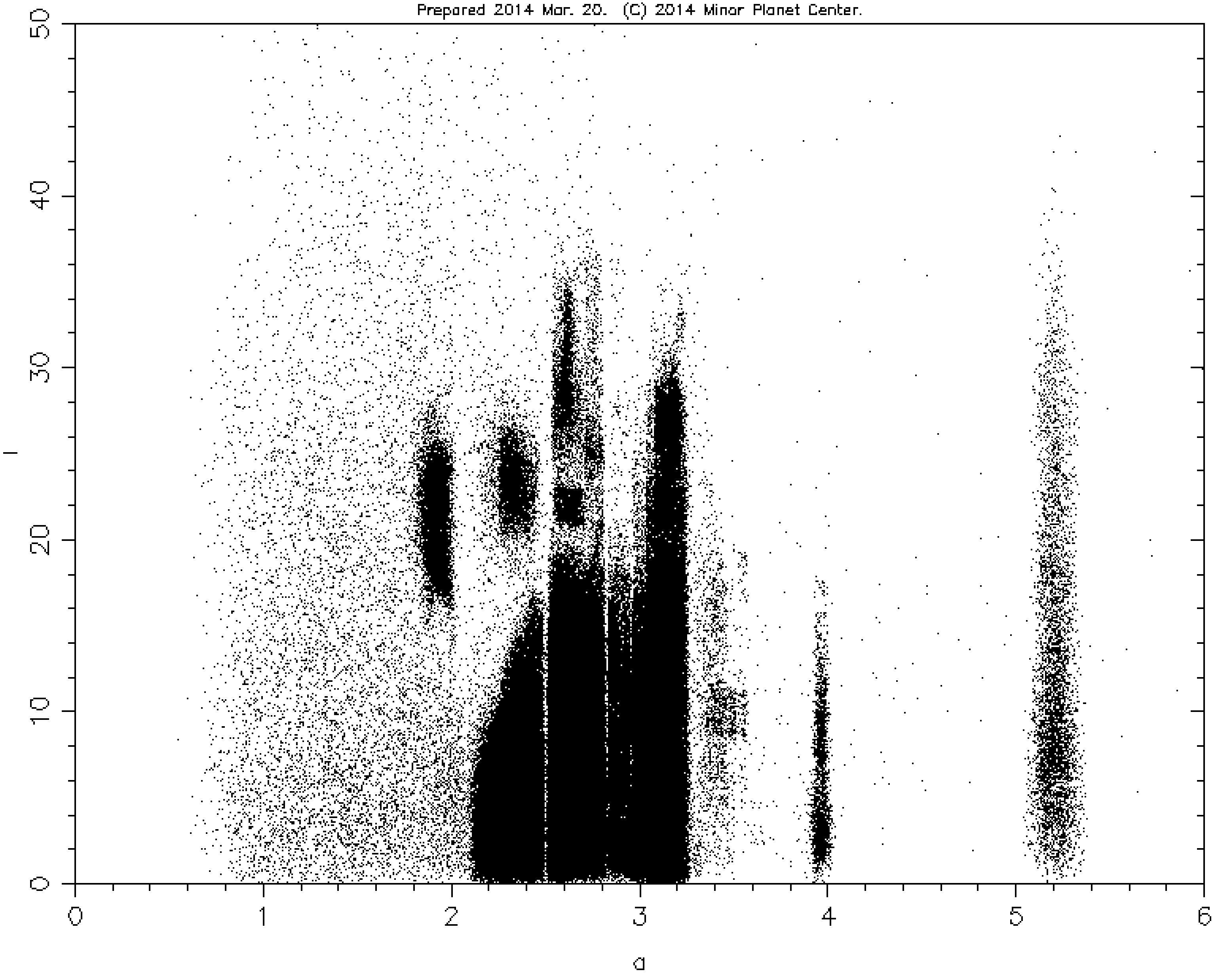

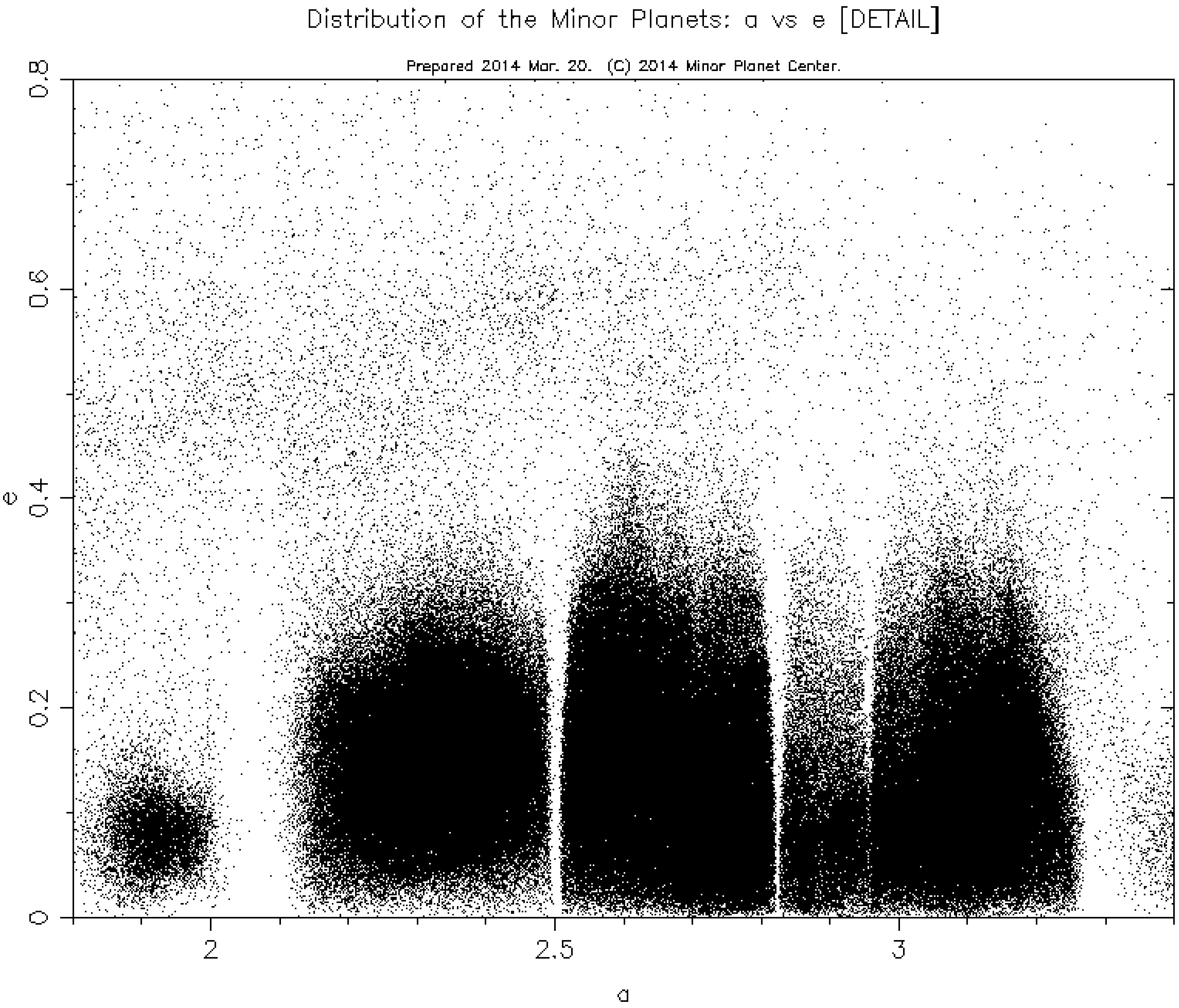
Distribution of the Minor Planets: a vs e [DETAIL]
Prepared 2014 Mar. 20. (C) 2014 Minor Planet Center.
e
0
0.2
0.4
0.6
0.8
2
2.5
3
a

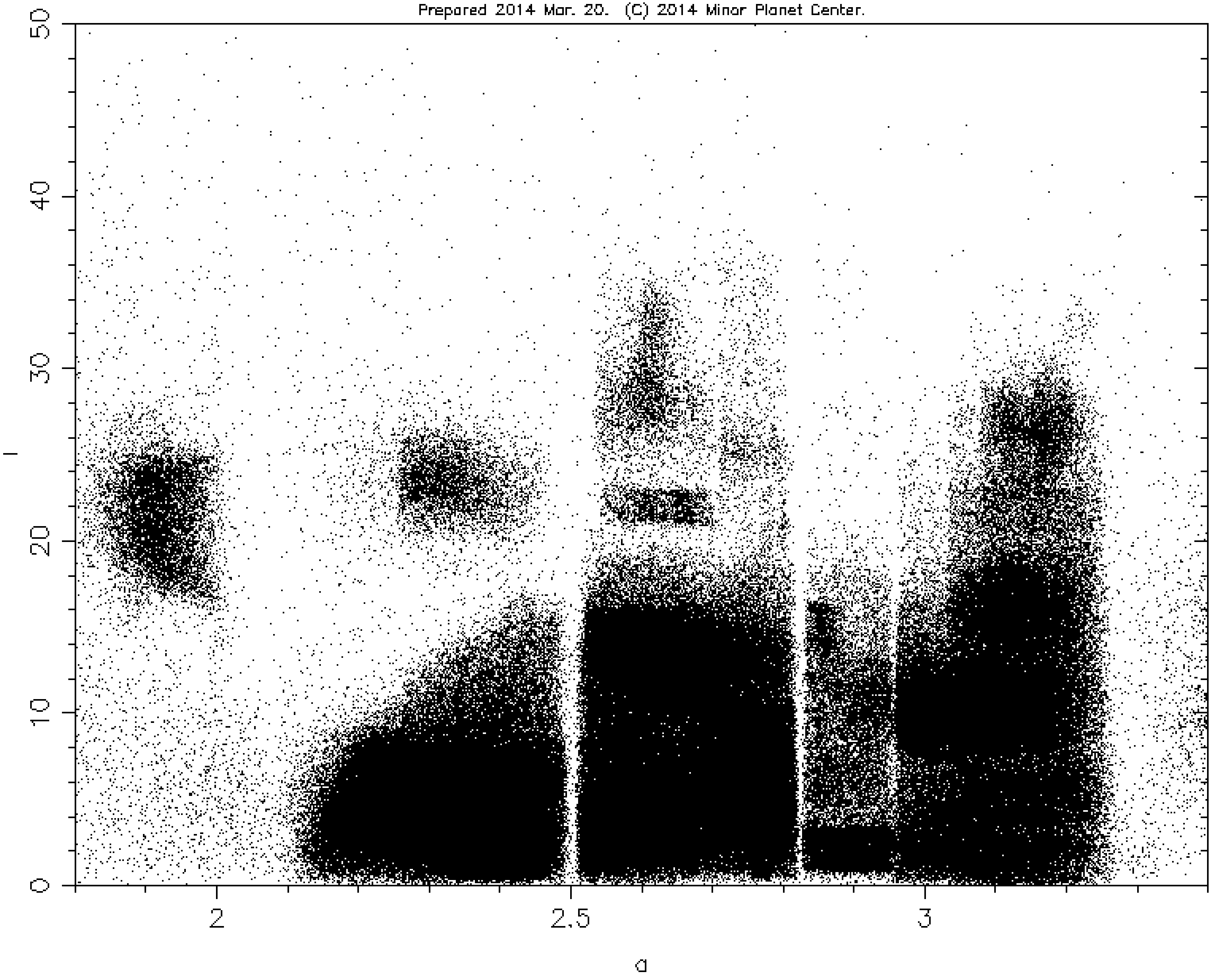

Distribution of the Minor Planets: a vs i [DETAIL]

Prepared 2014 Mar. 20. (C) 2014 Minor Planet Center.

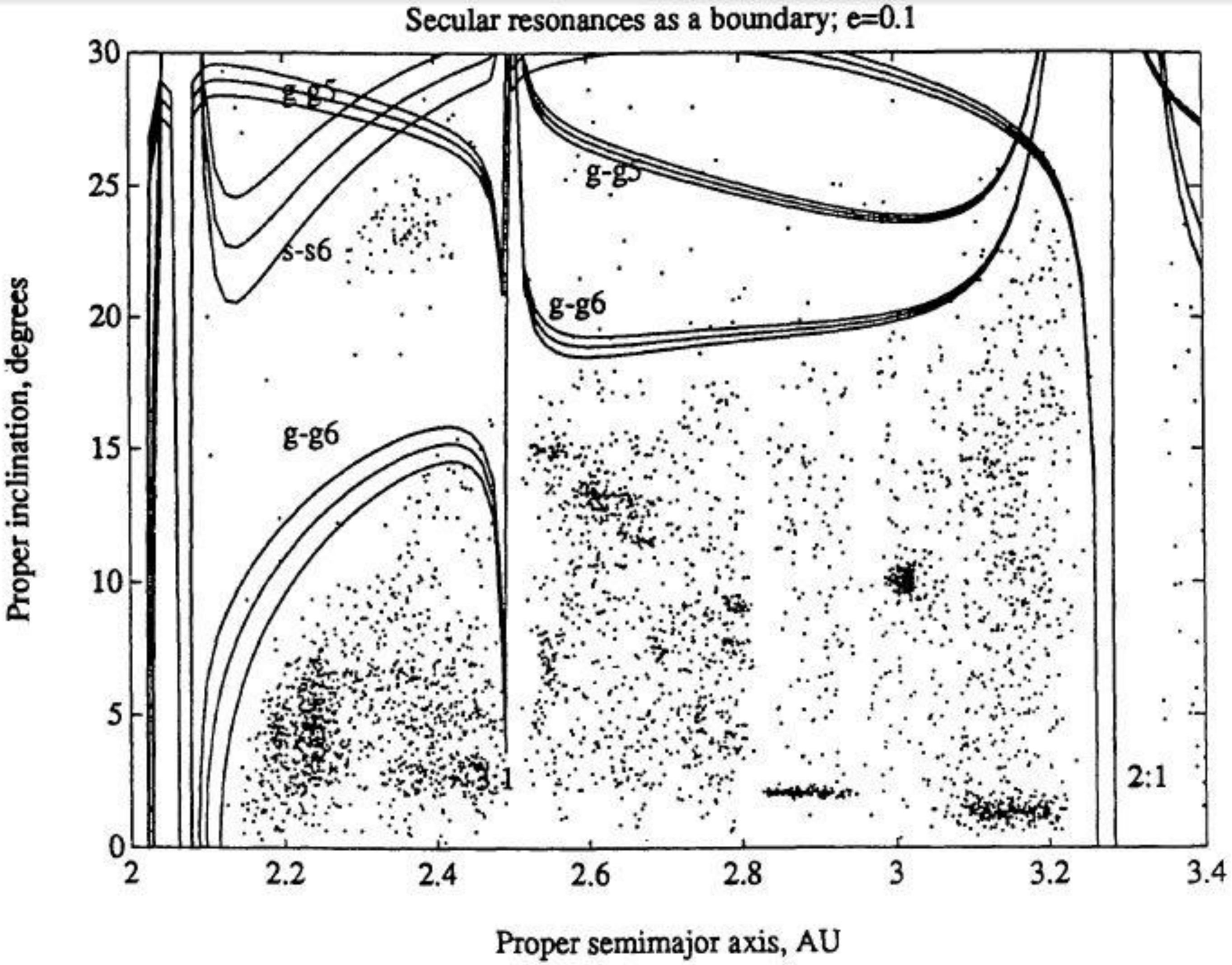

Fig. 1. The location of the main linear secular resonances for proper $e = 0.1$ according to Milani and Knežević (1990). The location of the resonances is strongly affected by the interaction with the mean motion resonances 3/1 and 2/1. The contour lines around the secular resonances correspond to a width of +/− 1"/yr.

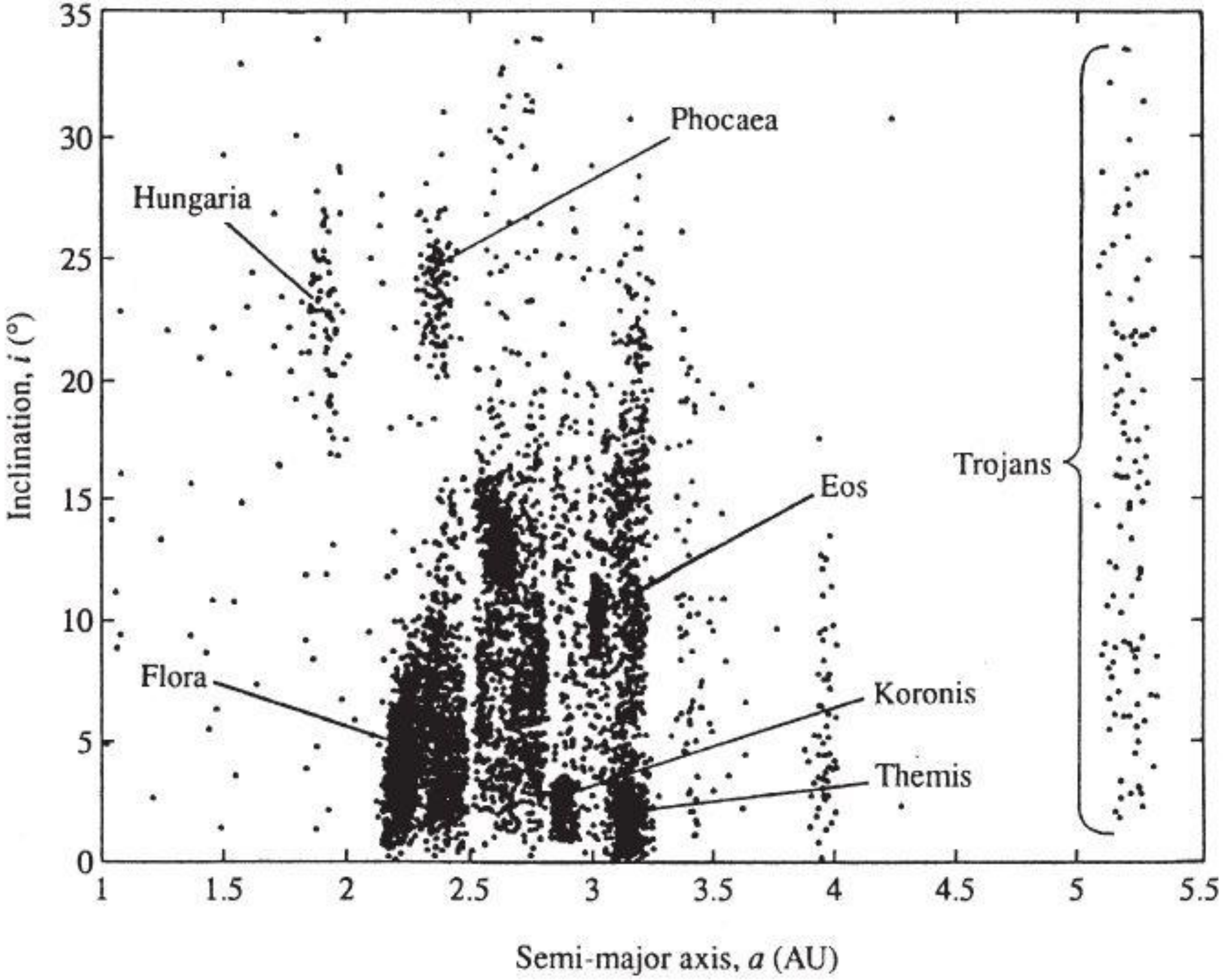

Figure 12.8 This plot of the inclination versus semimajor axis of MBAs reveals many groupings of asteroids with similar proper orbital elements. These groups, or asteroid families, represent remnants of collisionally disrupted large asteroids. (Kowal 1996)

Distribution of the Minor Planets: Longitude of Perihelion vs e

Prepared 2014 Mar. 20. (C) 2014 Minor Planet Center.

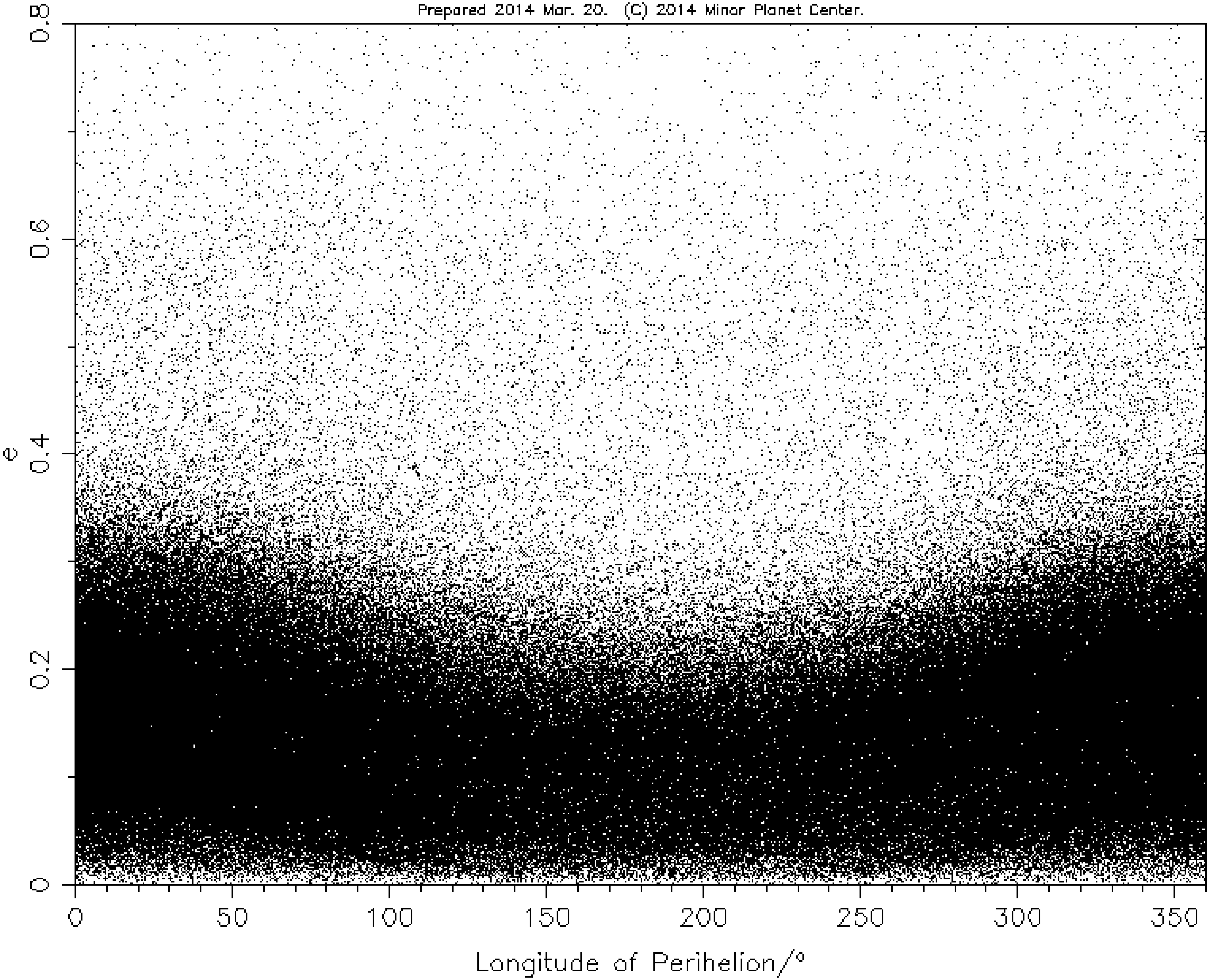

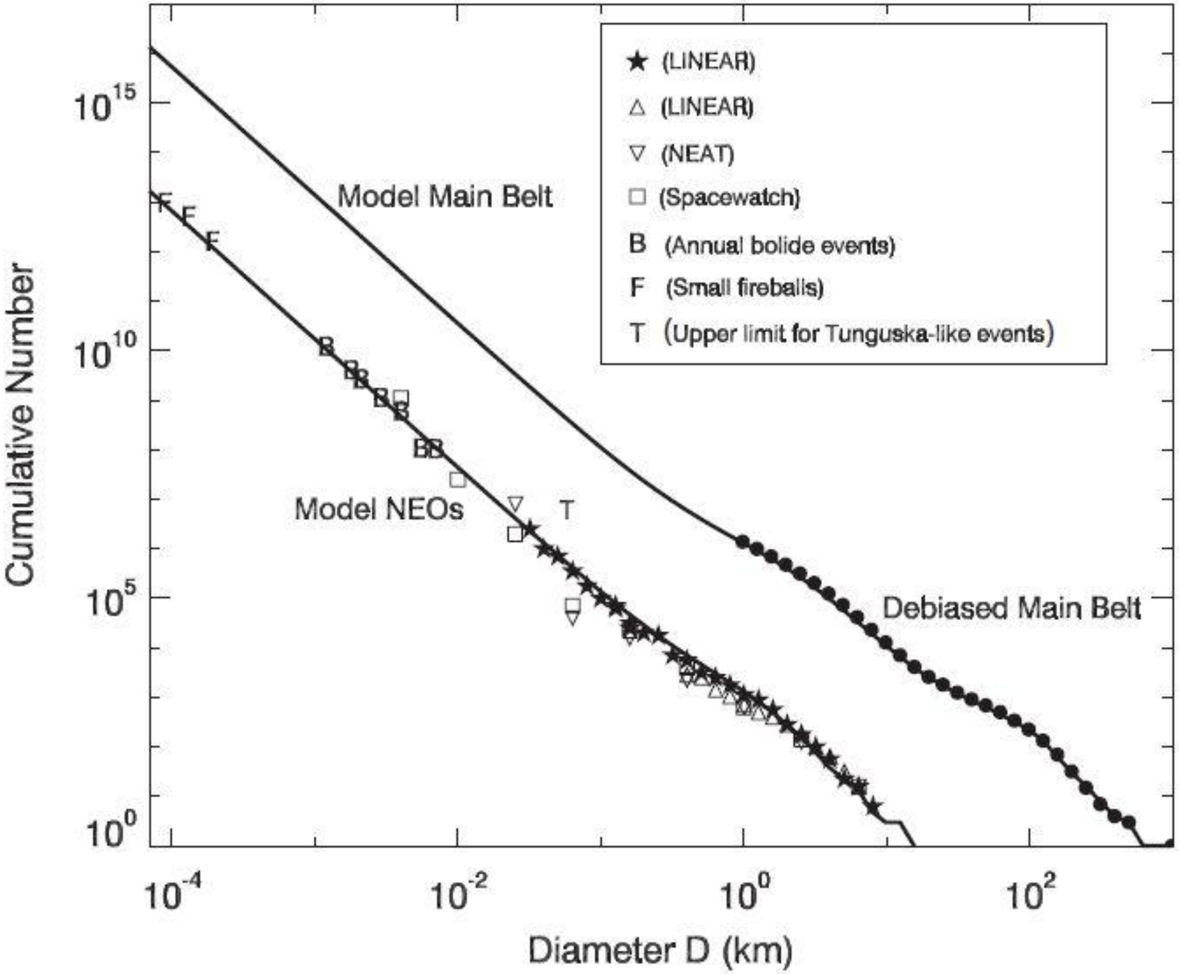

Figure 12.7 Comparison of a model of the dynamical evolution (*solid lines*) with the observationally debiased size distribution of MBAs and near-Earth objects (NEOs). Most bodies with $D \lesssim 100$ km are fragments (or fragments of fragments) derived from a limited number of breakups of bodies with $D \gtrsim 100$ km. The NEO model population is compared with estimates derived from telescopic surveys, spacecraft detections of bolide detonations in Earth's atmosphere and photographs of fireballs. The symbol T is an estimate on the upper limit of 50 m NEOs, derived from the uniqueness of the Tunguska airblast in 1908 (§6.4.5). (Adapted from Bottke et al. 2005b)

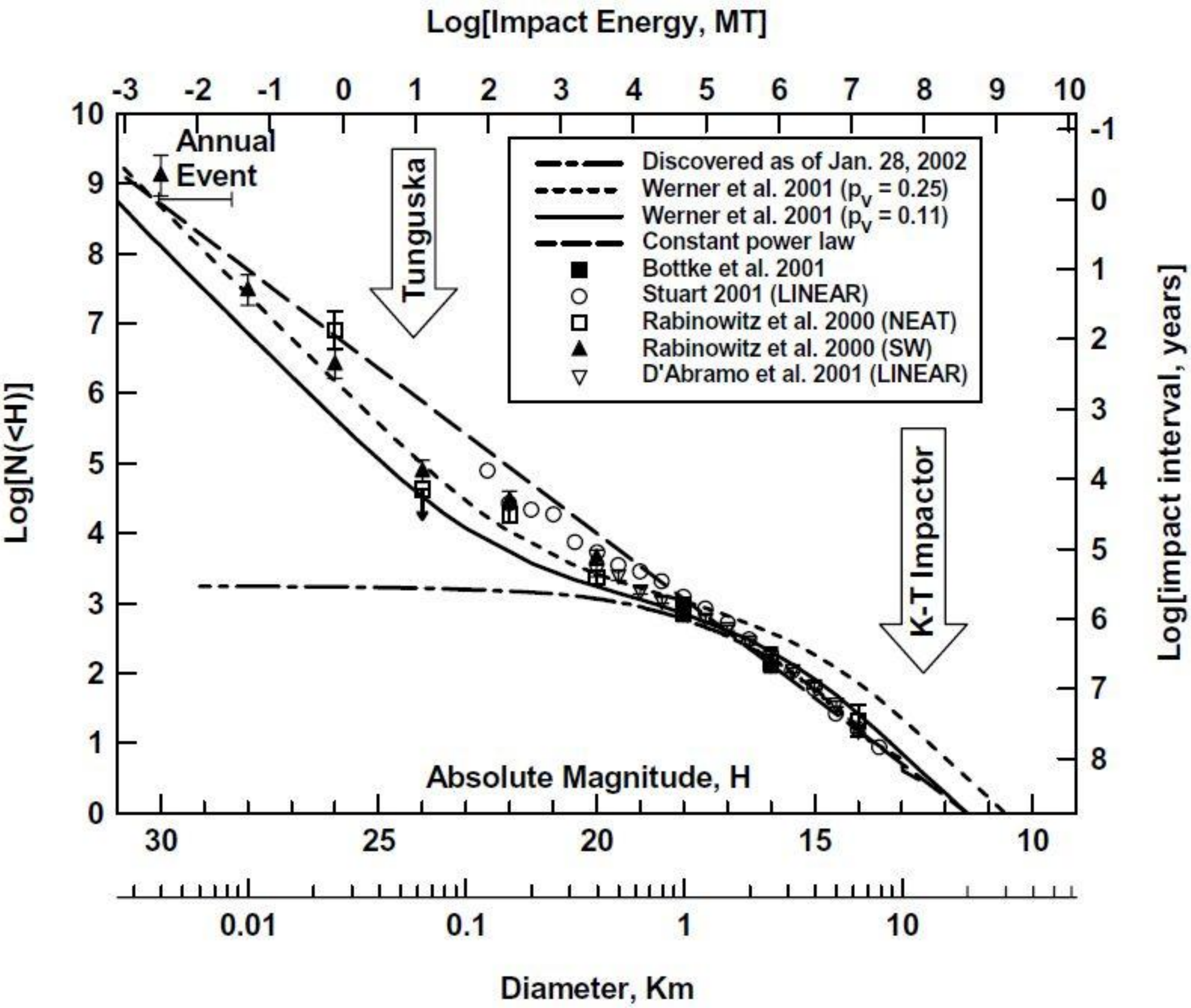
Log[Impact Energy, MT]
-3
-2
-1
0
1
2
3
4
5
6
7
8
9
10
Log[N(<H)]
0
1
2
3
4
5
6
7
8
9
10
Log[impact interval, years]
-1
0
1
2
3
4
5
6
7
8
Annual Event
Tunguska
K-T Impactor
Discovered as of Jan. 28, 2002
Werner et al. 2001 (p_V = 0.25)
Werner et al. 2001 (p_V = 0.11)
Constant power law
Bottke et al. 2001
Stuart 2001 (LINEAR)
Rabinowitz et al. 2000 (NEAT)
Rabinowitz et al. 2000 (SW)
D'Abramo et al. 2001 (LINEAR)
Absolute Magnitude, H
30
25
20
15
10
0.01
0.1
1
10
Diameter, Km

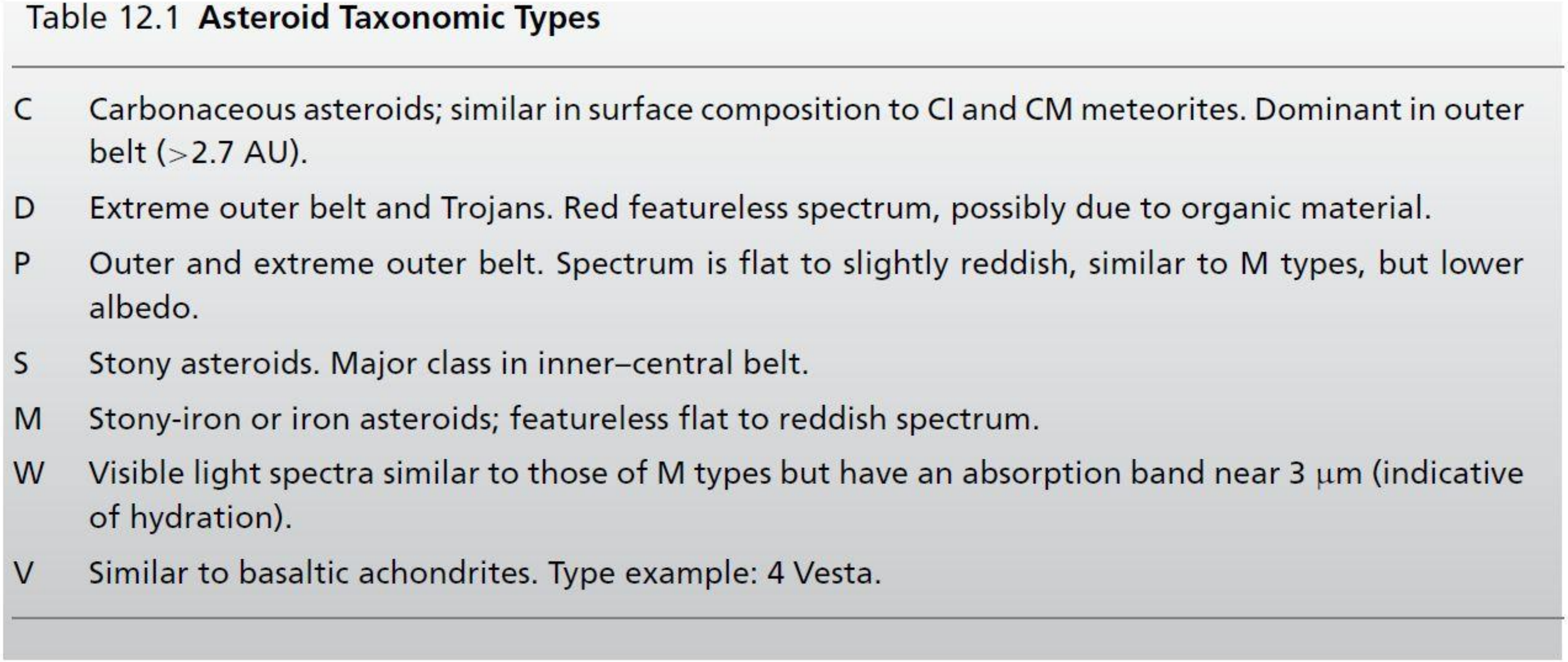

Table 12.1 **Asteroid Taxonomic Types**

C	Carbonaceous asteroids; similar in surface composition to CI and CM meteorites. Dominant in outer belt (>2.7 AU).
D	Extreme outer belt and Trojans. Red featureless spectrum, possibly due to organic material.
P	Outer and extreme outer belt. Spectrum is flat to slightly reddish, similar to M types, but lower albedo.
S	Stony asteroids. Major class in inner–central belt.
M	Stony-iron or iron asteroids; featureless flat to reddish spectrum.
W	Visible light spectra similar to those of M types but have an absorption band near 3 μm (indicative of hydration).
V	Similar to basaltic achondrites. Type example: 4 Vesta.

Typical asteroid spectra

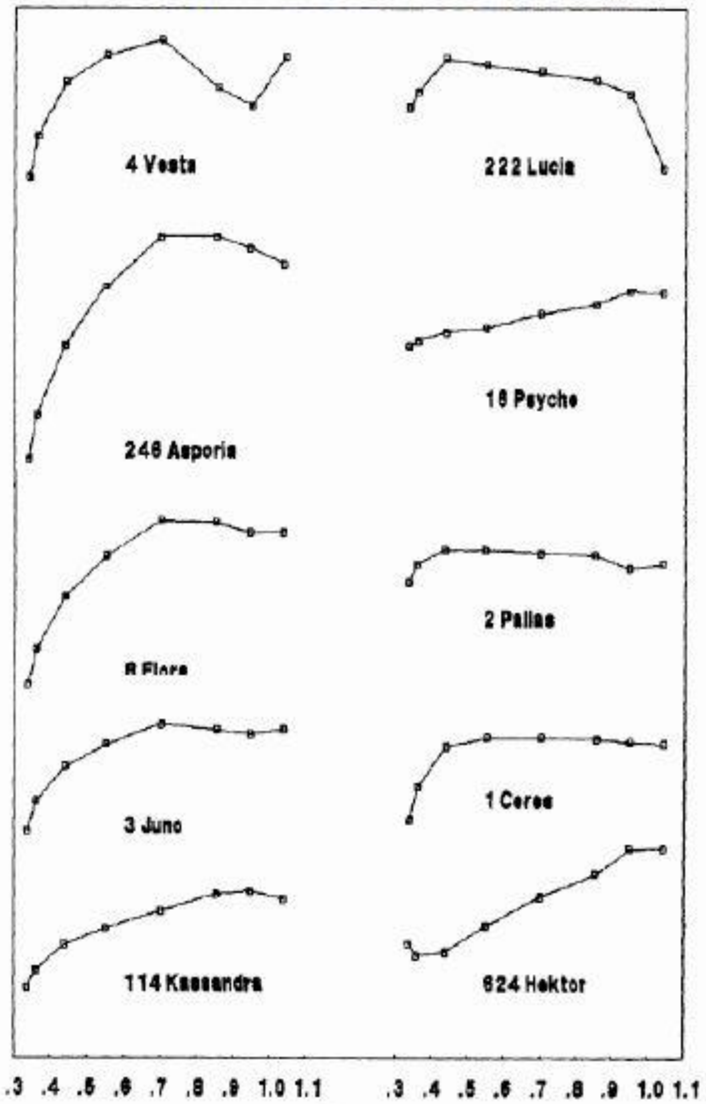

Figure 2. Reflectance spectra of the classes described by the taxonomy introduced in this paper.

lab spectra of minerals expected

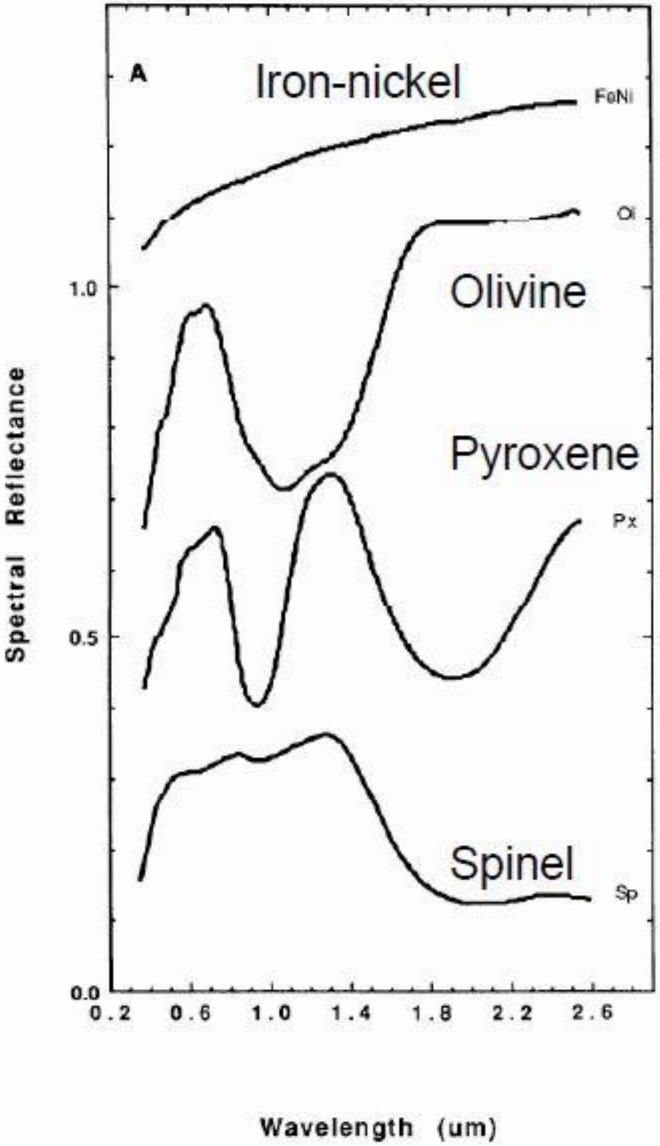

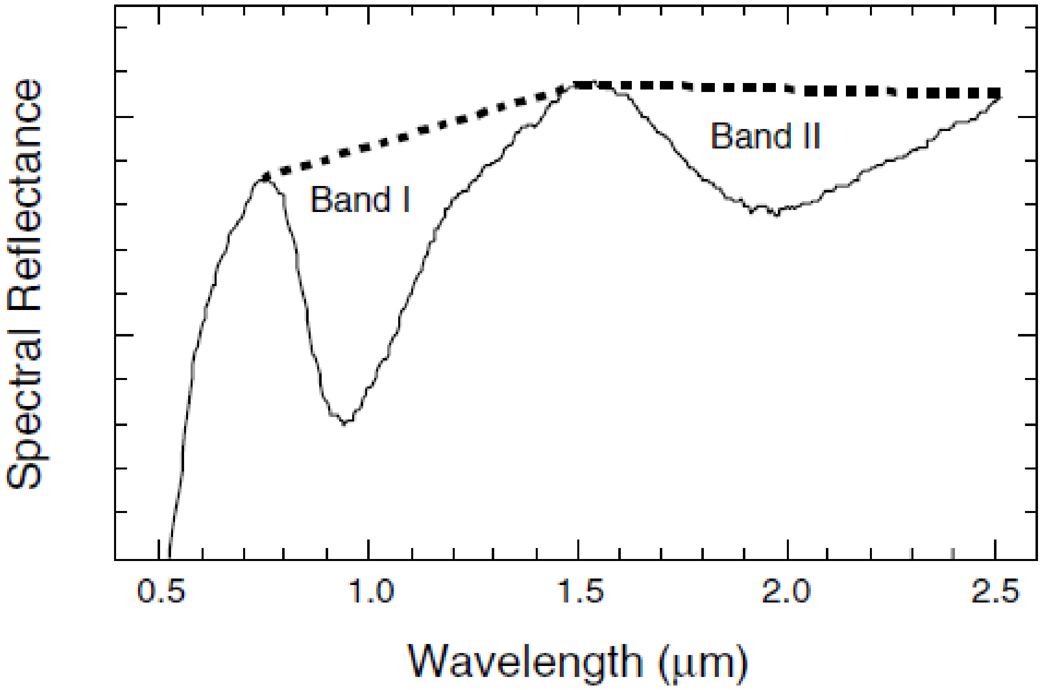

Fig. 3. The spectral reflectance curve of an olivine-pyroxene dominated meteorite sample (average LL3 chondrite). Band I and Band II are indicated. The band areas are the areas between the spectral curve and linear continua (shown as dashed lines) fitted tangent to the spectral curve at the edge of the absorption feature. The band area ratio (BAR) is the ratio of the area of Band II to that of Band I (BII/BI). Band centers are calculated by dividing out the linear continuum (to remove the effects of spectral slope) and fitting a polynomial function to the wavelength interval around the minimum in the ratioed curve.

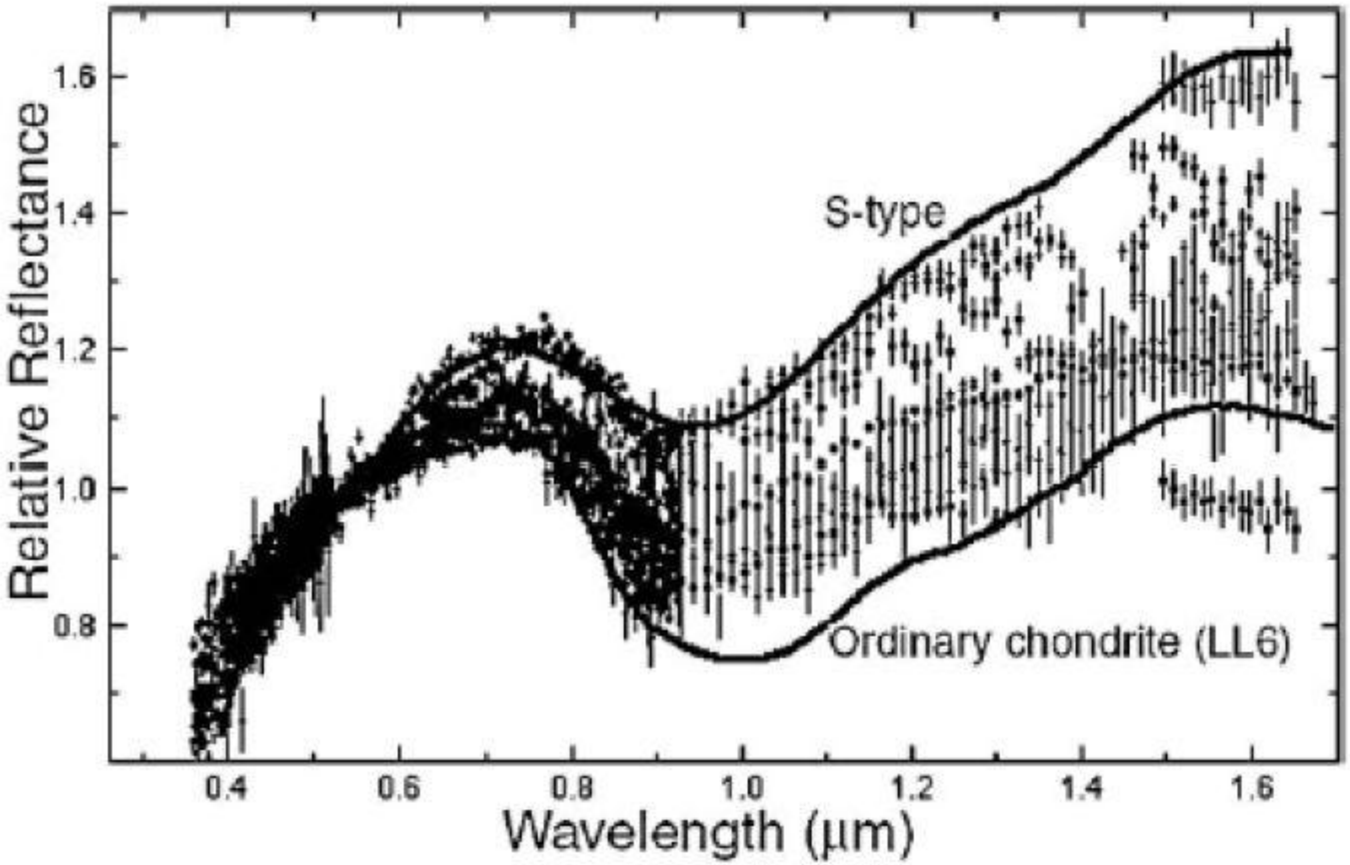

Figure 5 A continuum of reflectance spectra range from S-types to Q-types. More asteroids were observed out to 0.9 μm, and only a few to longer wavelengths. (Courtesy R. Binzel.)

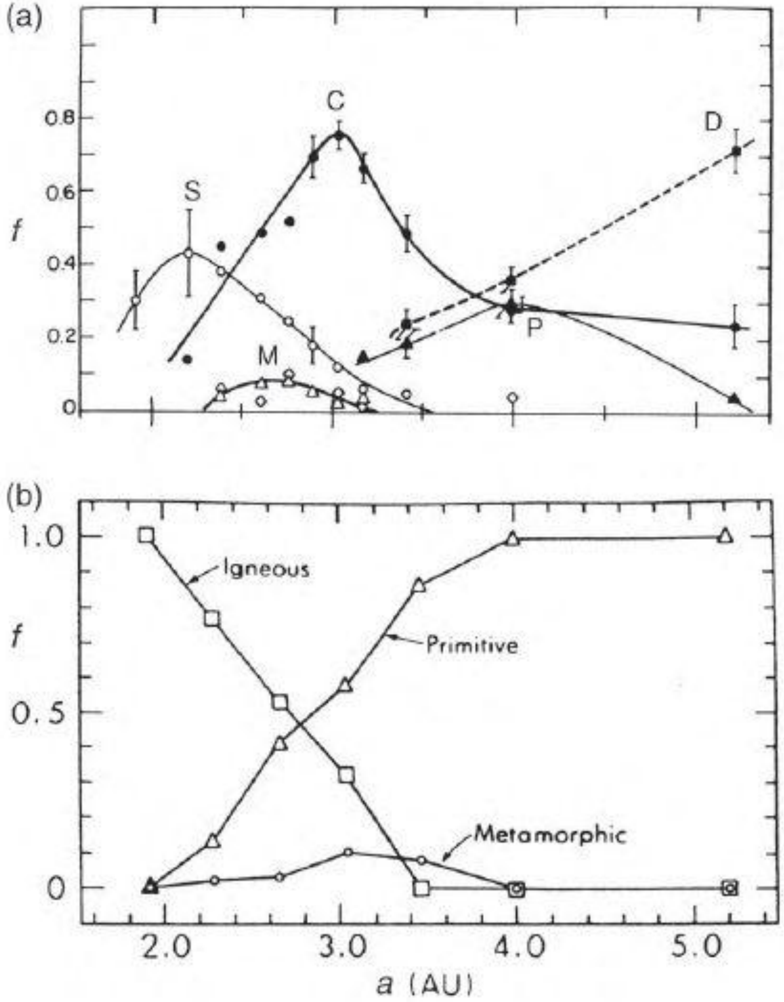

Figure 12.16 (a) Graph showing the relative distribution of the asteroid taxonomic classes as a function of heliocentric distance. The classes S, C, M, P and D are shown. Smooth curves are drawn through the data points for clarity. (Adapted from Gradie et al. 1989) (b) Distribution of igneous, primitive and metamorphic classes as a function of heliocentric distance. (This figure assumes that S-type asteroids are igneous bodies.) (Adapted from Bell et al. 1989)

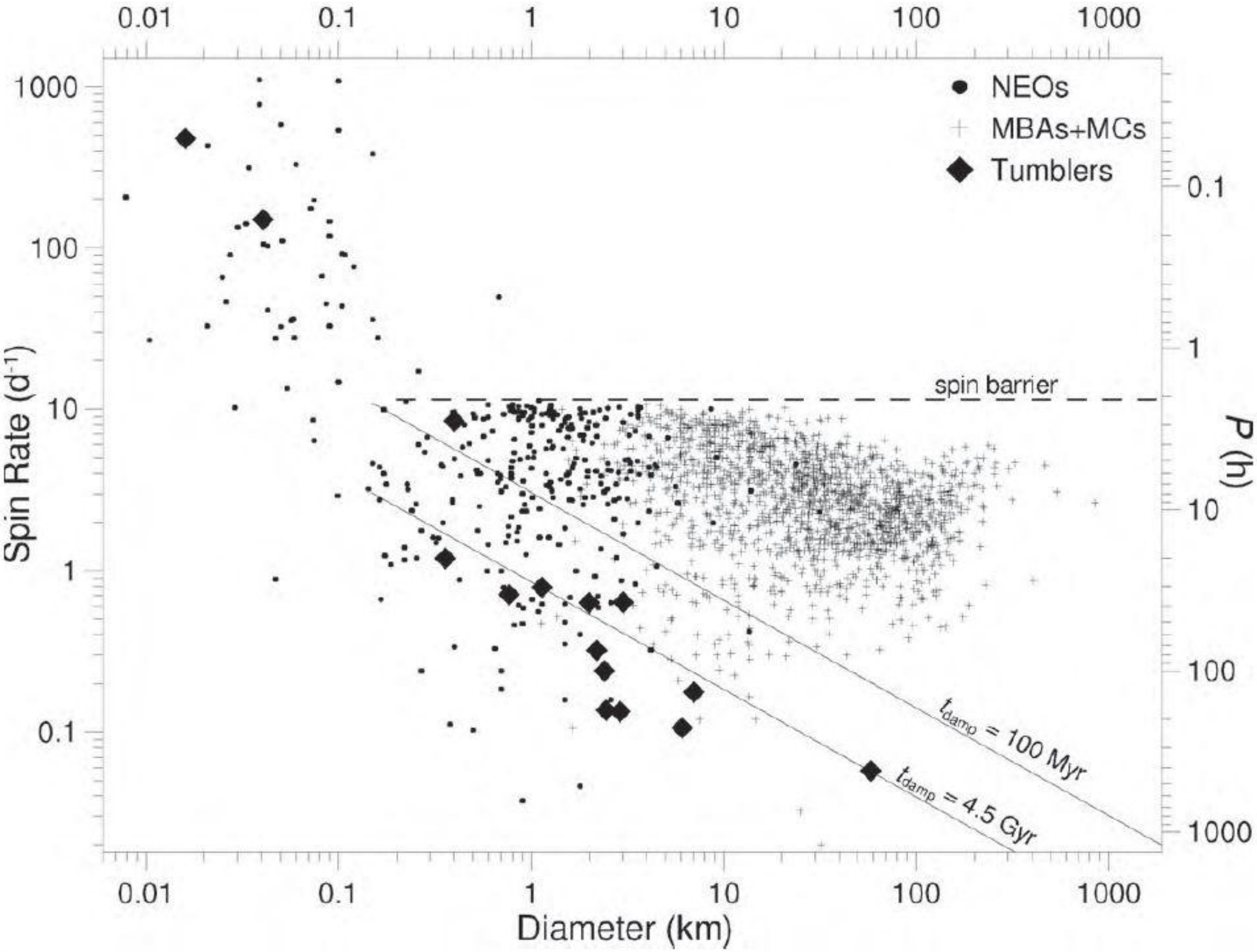

Figure 12.15 Plot of the rotational period (*right vertical axis*) and spin rate (*left vertical axis*) versus diameter for main belt (MBA) and Mars-crossing (MC) asteroids, near-Earth objects (NEO) and tumbling asteroids. The *dashed line* denotes the maximum rotation rate for objects of density 3000 kg m^{-3} that are bound gravitationally. (Adapted from Pravec et al. 2007)

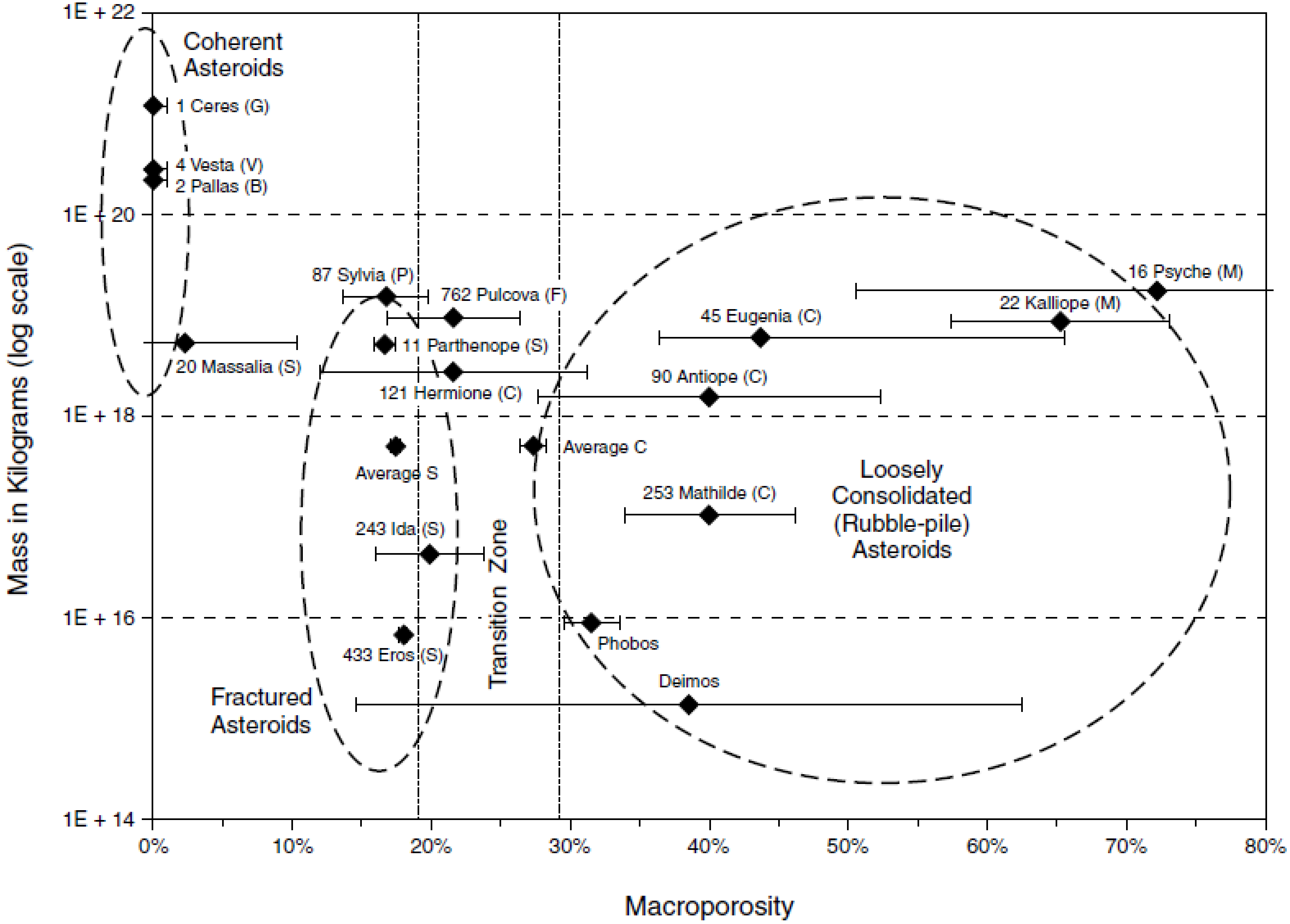

Fig. 4. Asteroid macroporosity estimated by subtracting the average porosity of asteroid's meteorite analogue from the bulk porosity shown in Fig. 3. Since microporosity probably does not seriously effect the structural integrity of asteroids, this is a direct estimate of the large-scale fractures and voids that determine the asteroid's internal structure.

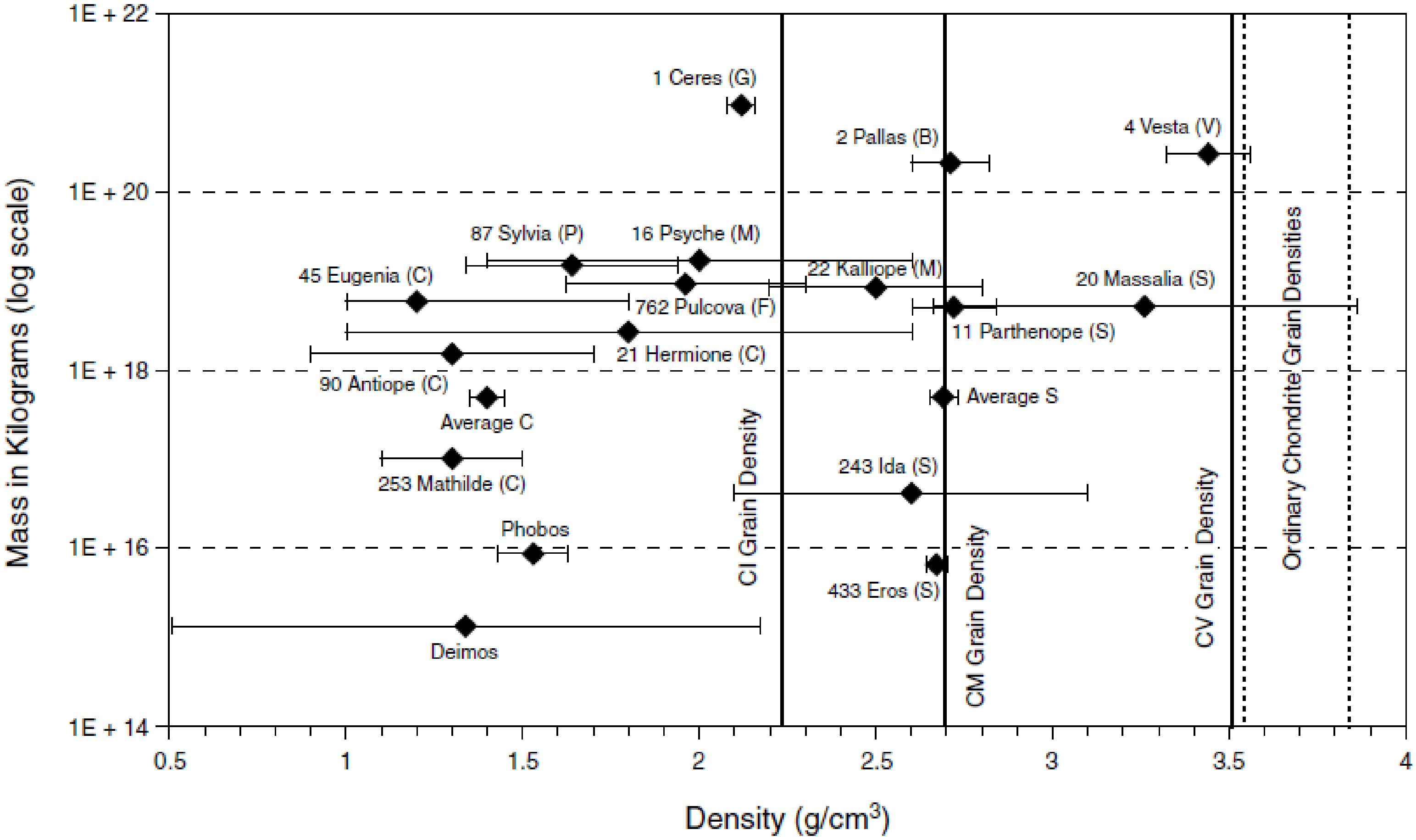

Fig. 1. Bulk densities of measured asteroids with the grain densities of common meteorites for comparison. Also included in the plot are the asteroidlike moons of Mars, Phobos and Deimos, as well as estimates for the average C- and S-type asteroids (*Standish,* 2001). Several asteroids in Table 1 with large error bars have been left off the plot for clarity.

Largest known trans-Neptunian objects (TNOs)

Table E.7 **Seven Largest Distant Minor Planets (Known as of 2012; $a > 6$ AU)**

#	Name	Provisional Name	Dynamical Class	M_V	Radius[a] (km)	A_0[b]	a (AU)	e	i (deg)	P_{orb} (yr)	P_{rot} (hr)
136199	Eris	2003 UB_{313}	SDO	−1.17	1163 ± 6	0.96	67.728	0.44	43.97	557.5	
134340	Pluto		RKBO	−0.7	1153 ± 10	0.5[b]	39.482	0.249	17.14	247.7	153.3
136472	Makemake	2005 FY_9	RKBO	−0.48	710 ± 30	0.77	45.678	0.16	29.00	308.0	7.77
136108	Haumea	2003 EL_{61}	SDO	0.18	675 ± 125	0.84	43.329	0.19	28.21	284.8	3.92
225088		2007 OR_{10}	SDO	2.0	640 ± 110	0.19	67.21	0.50	30.7	551.0	
	Charon		Moon	1.3	606 ± 1.5	0.375	39.482	0.249	17.14	247.7	153.3
90377	Sedna	2003 VB_{12}	IOC	1.56	<800	>0.16	489.6	0.84	11.93	10 718	10.27

Data from Stansberry et al. (2008), Brown et al. (2010), Sicardy et al. (2011), Santos-Sanz et al. (2012) and http://ssd.jpl.nasa.gov/.

IOC, inner Oort cloud; resonant Kuiper belt object; SDO: scattered disk object.

[a] For all bodies, except Pluto/Charon and Eris, the radius and albedo were derived from Spitzer and Herschel (thermal IR) data.

[b] Changes with season between 0.44 and 0.61 as a consequence of variations in ice cover.

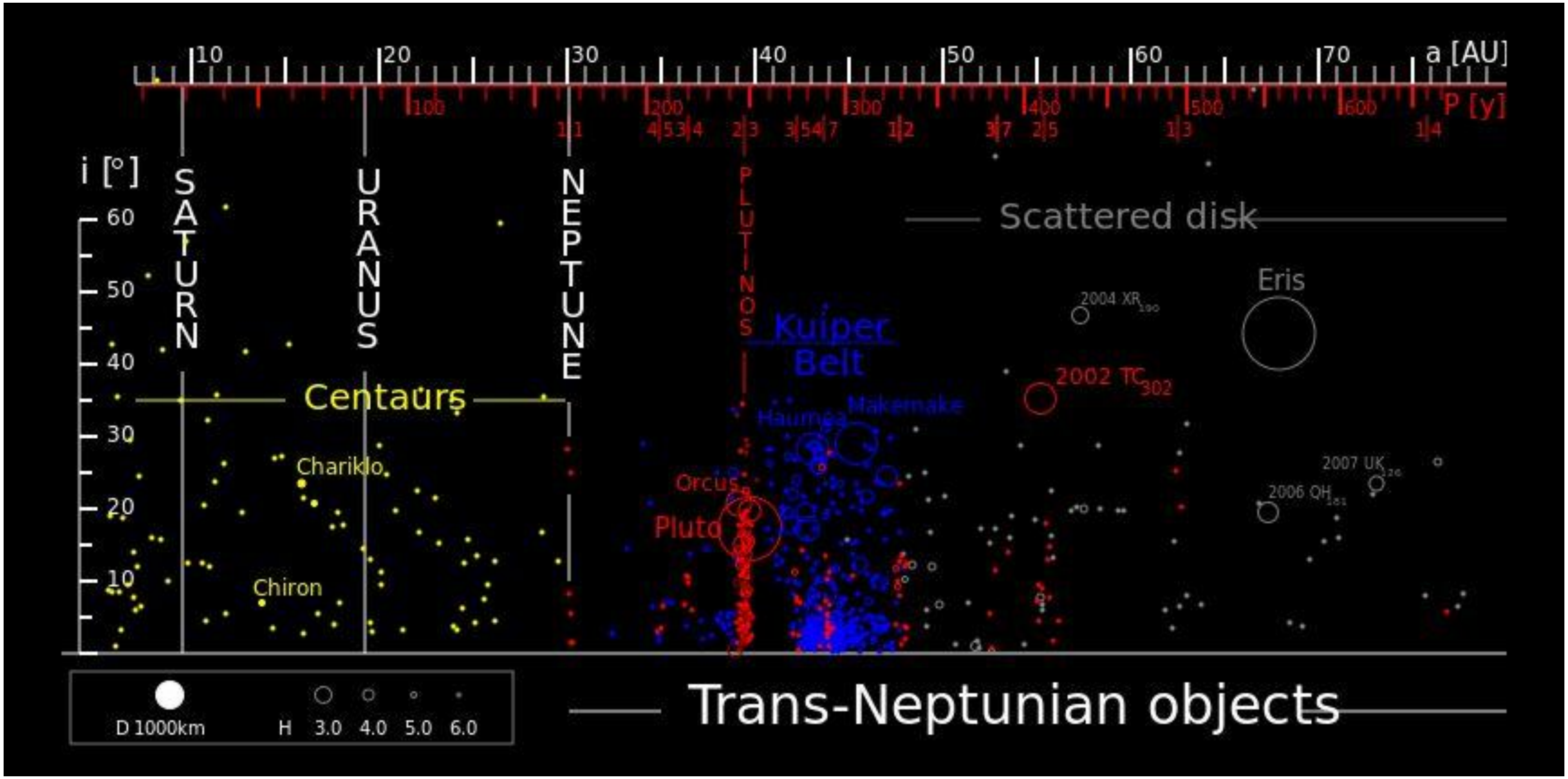
a [AU]
10
20
30
40
50
60
70
P [y]
100
200
300
400
500
600
1:1
4:5
3:4
2:3
3:5
4:7
1:2
3:7
2:5
1:3
1:4
i [°]
60
50
40
30
20
10
SATURN
URANUS
NEPTUNE
PLUTINOS
Scattered disk
Centaurs
Kuiper Belt
Eris
2004 XR190
2002 TC302
Haumea
Makemake
Orcus
Pluto
Chariklo
Chiron
2007 UK126
2006 QH181
D 1000km
H 3.0 4.0 5.0 6.0
Trans-Neptunian objects

Centauros y TNOs (junio 2014)

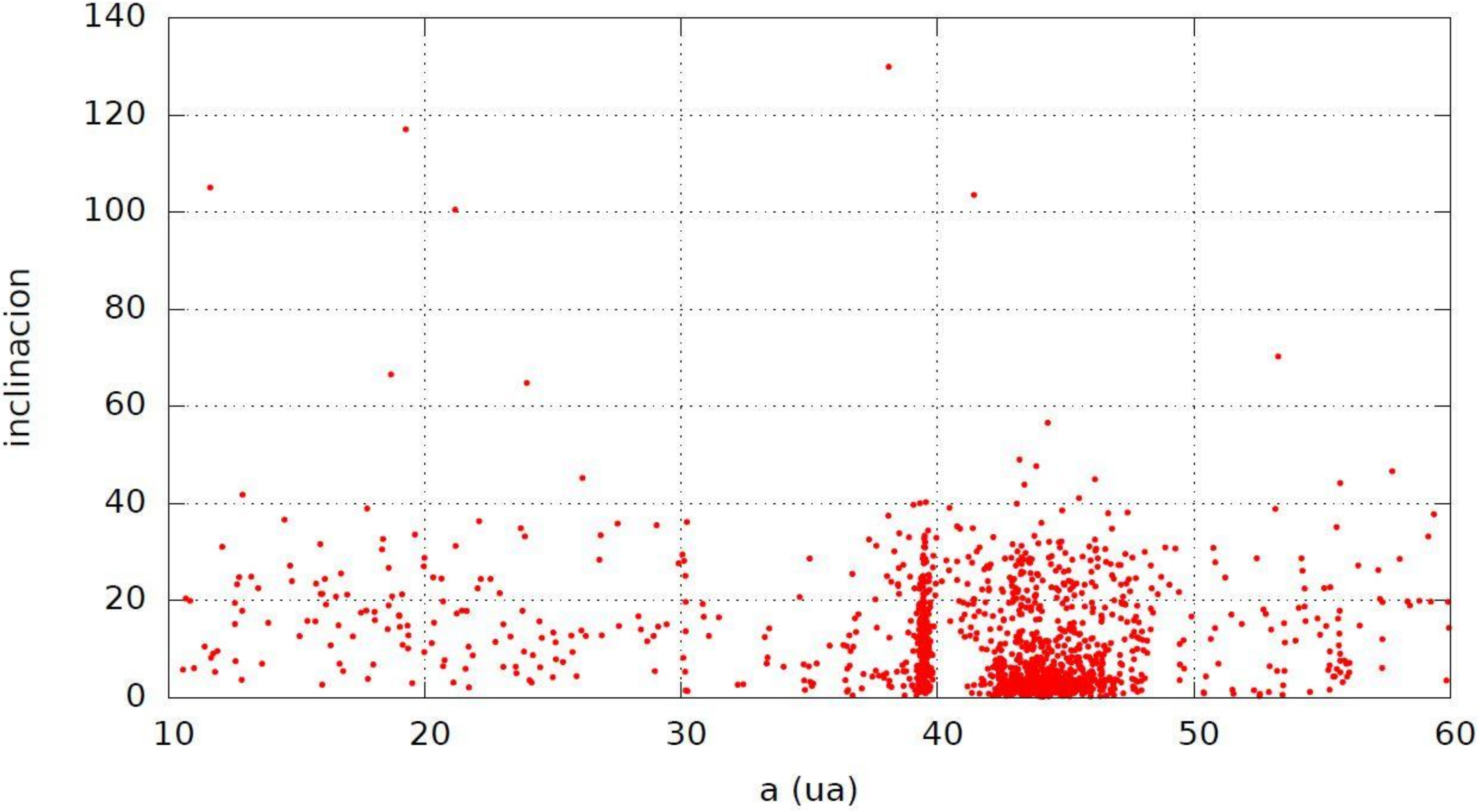

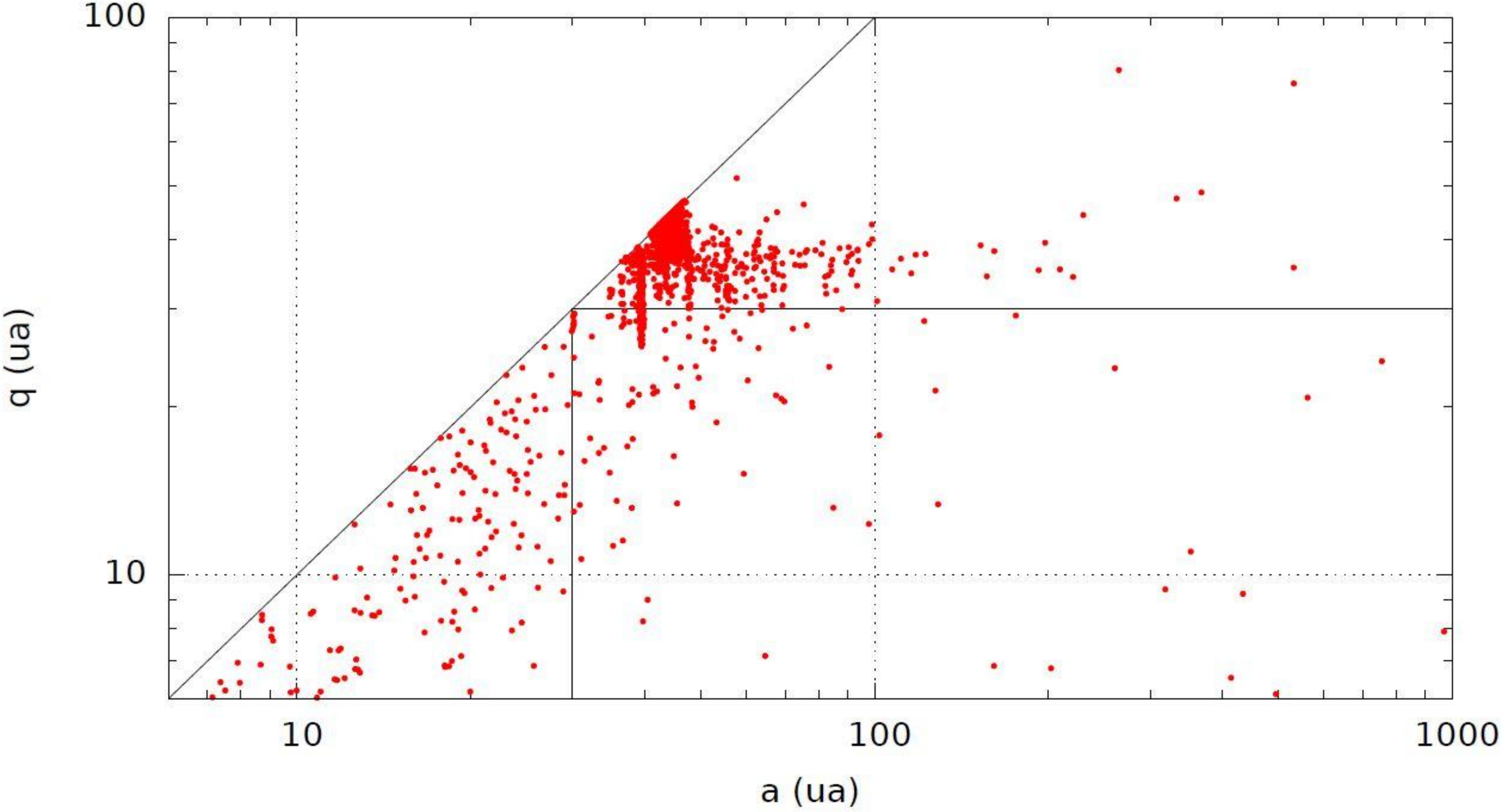

1716 objetos con q > 6 (junio 2014)

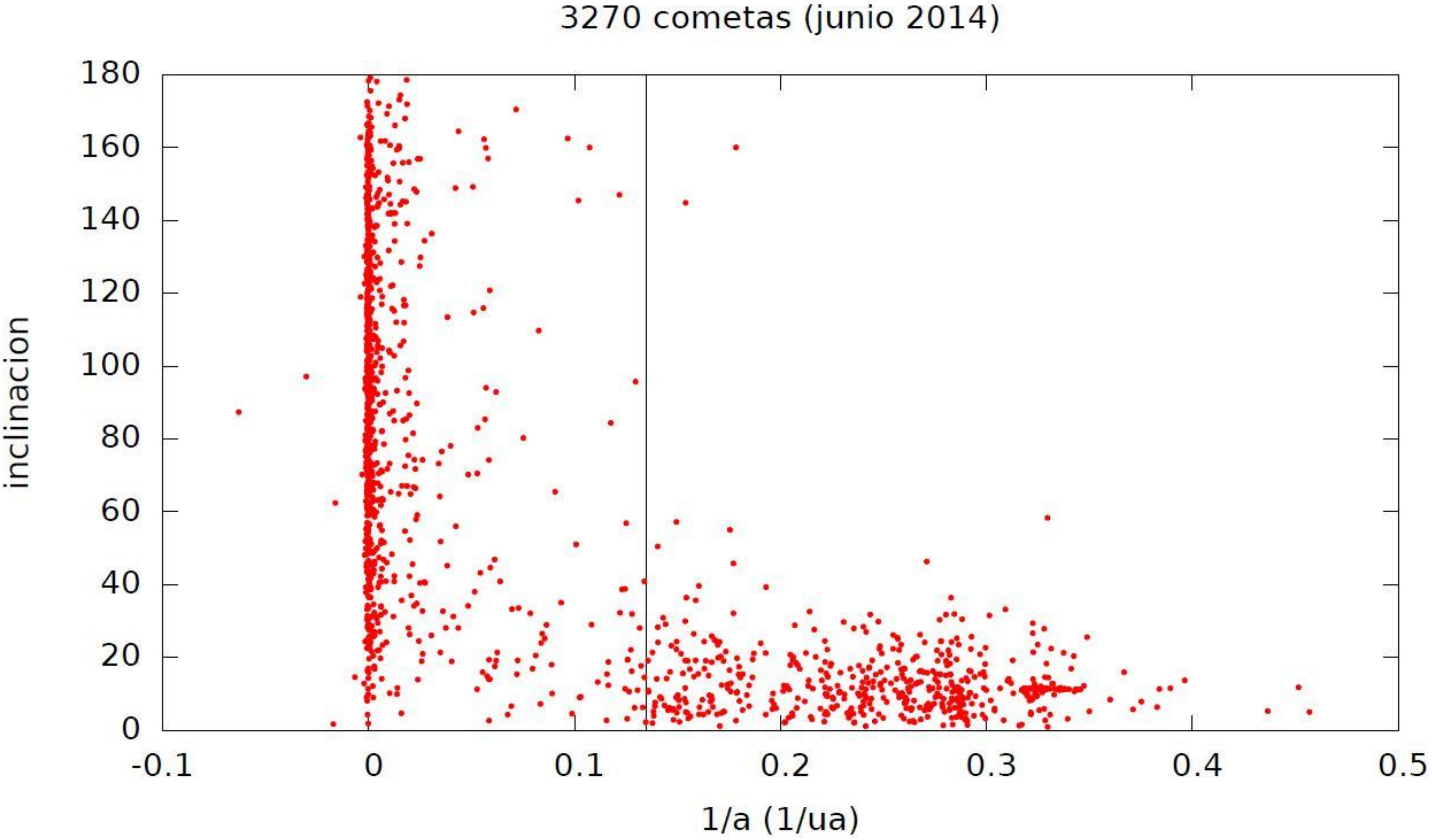
3270 cometas (junio 2014)
inclinacion
180
160
140
120
100
80
60
40
20
0
-0.1
0
0.1
0.2
0.3
0.4
0.5
1/a (1/ua)

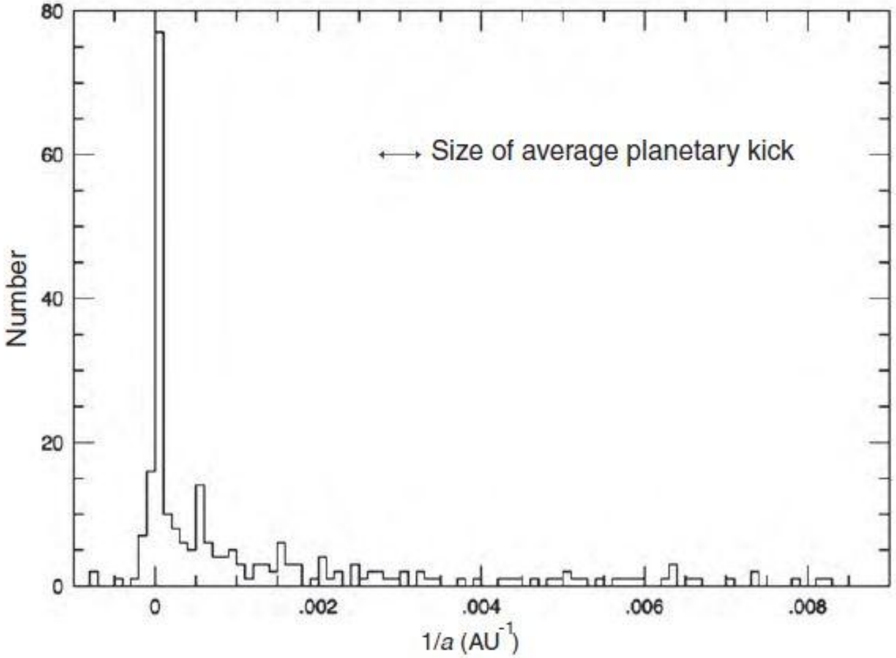

Figure 12.5 Distribution of the original (inbound) inverse semimajor axis, $1/a_0$, of all long-period comets in the 2003 version of Marsden and Williams's *Catalogue of Cometary Orbits*. The typical perturbation on $1/a$ due to a comet's passage through the inner Solar System is indicated on the graph. (Adapted from Levison and Dones 2007)

are almost certainly caused by errors in the calculation of the orbital elements

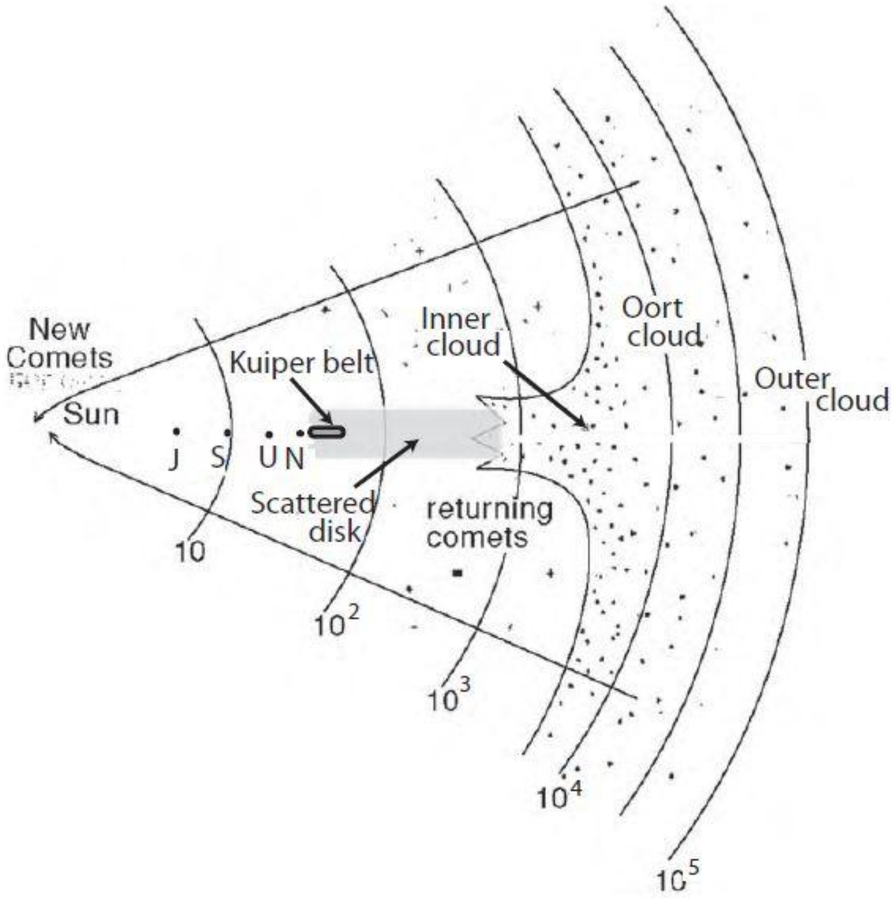

Figure 12.6 Schematic diagram of the structure of the inner and outer Oort cloud. The location of the giant plants and the Kuiper belt is indicated. Note that the distance scale is logarithmic. (Adapted from Levison and Dones 2007)

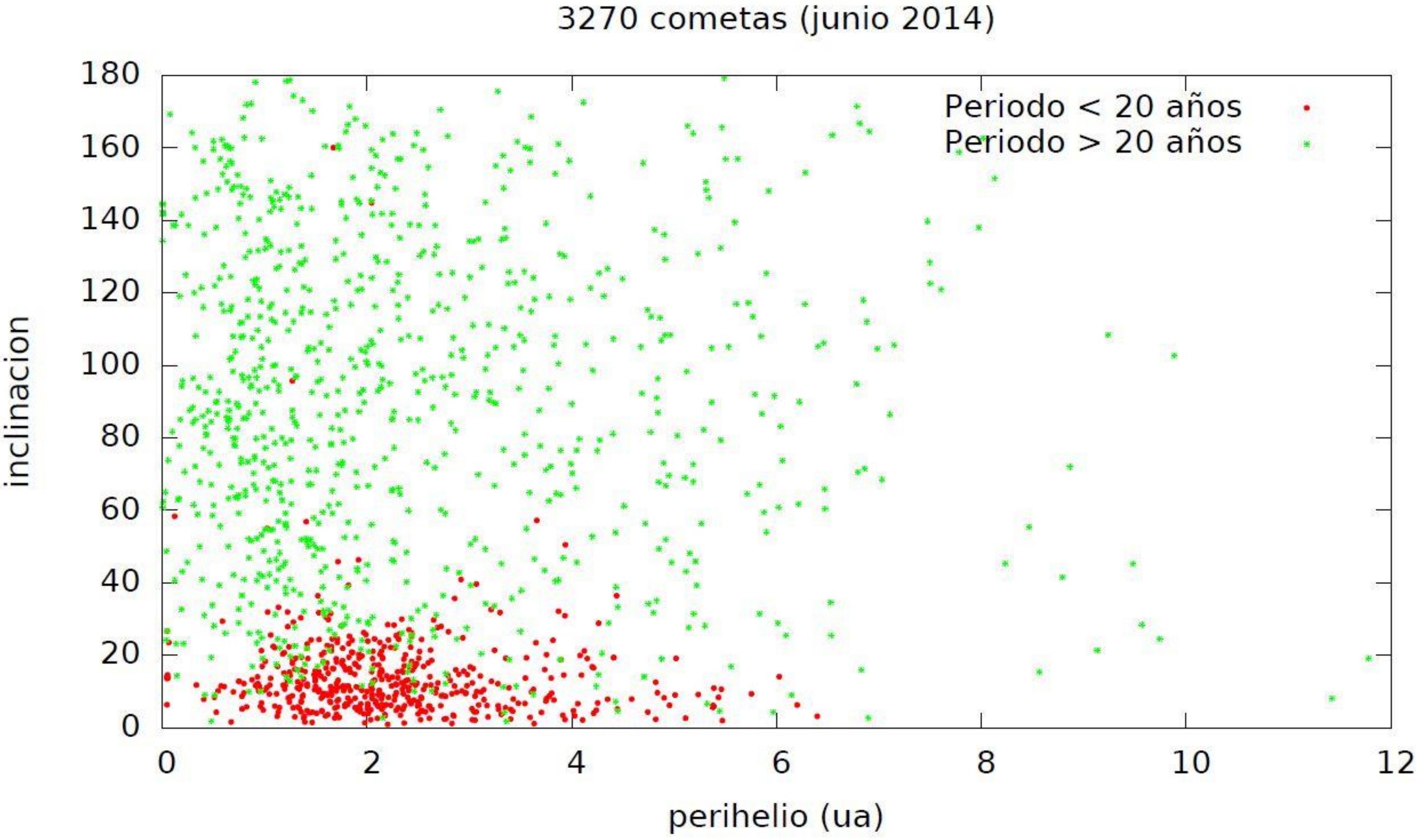
3270 cometas (junio 2014)
Periodo < 20 años
Periodo > 20 años
inclinacion
perihelio (ua)
0
20
40
60
80
100
120
140
160
180
0
2
4
6
8
10
12

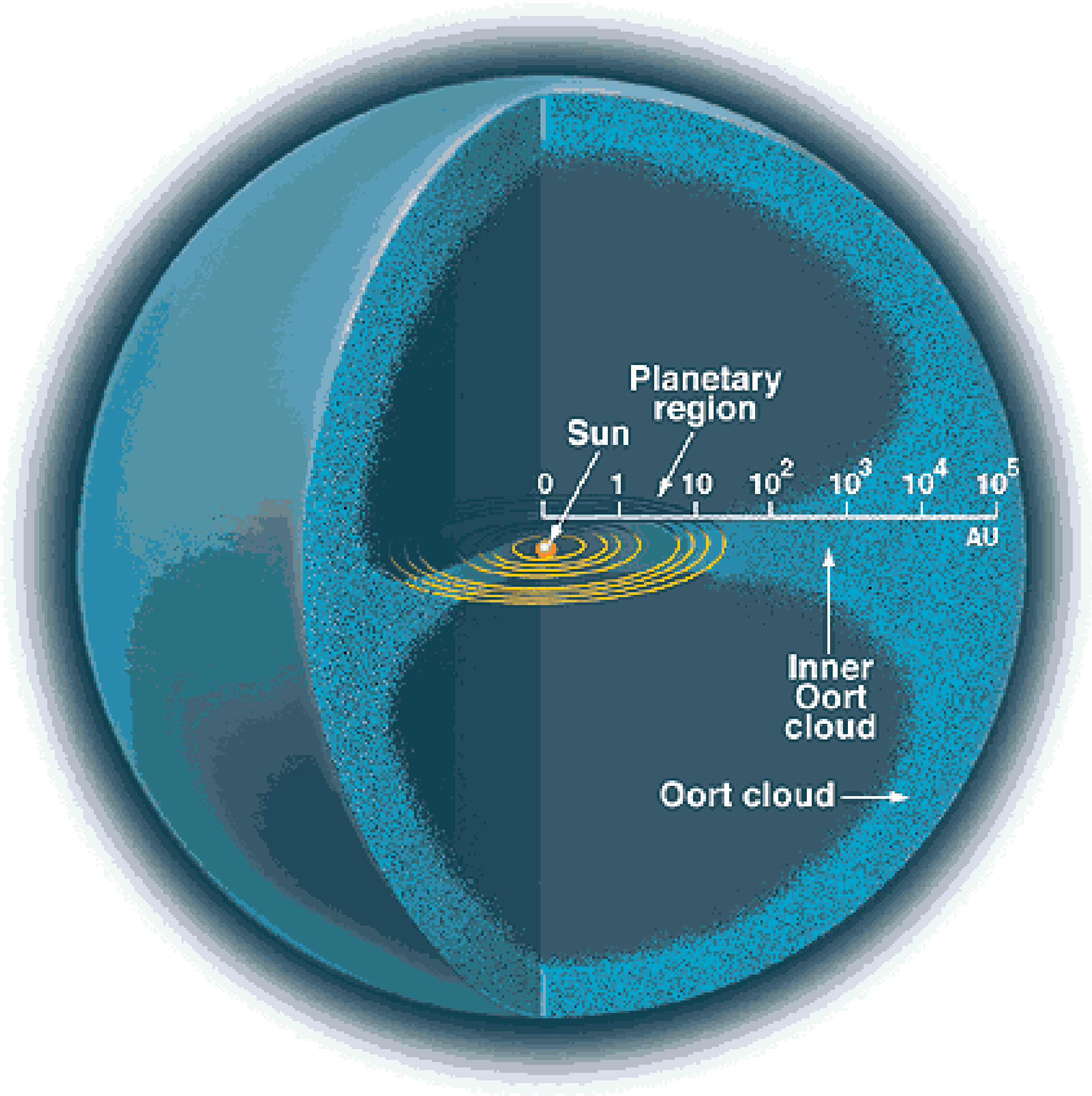
Planetary region
Sun
0
1
10
10²
10³
10⁴
10⁵
AU
Inner Oort cloud
Oort cloud

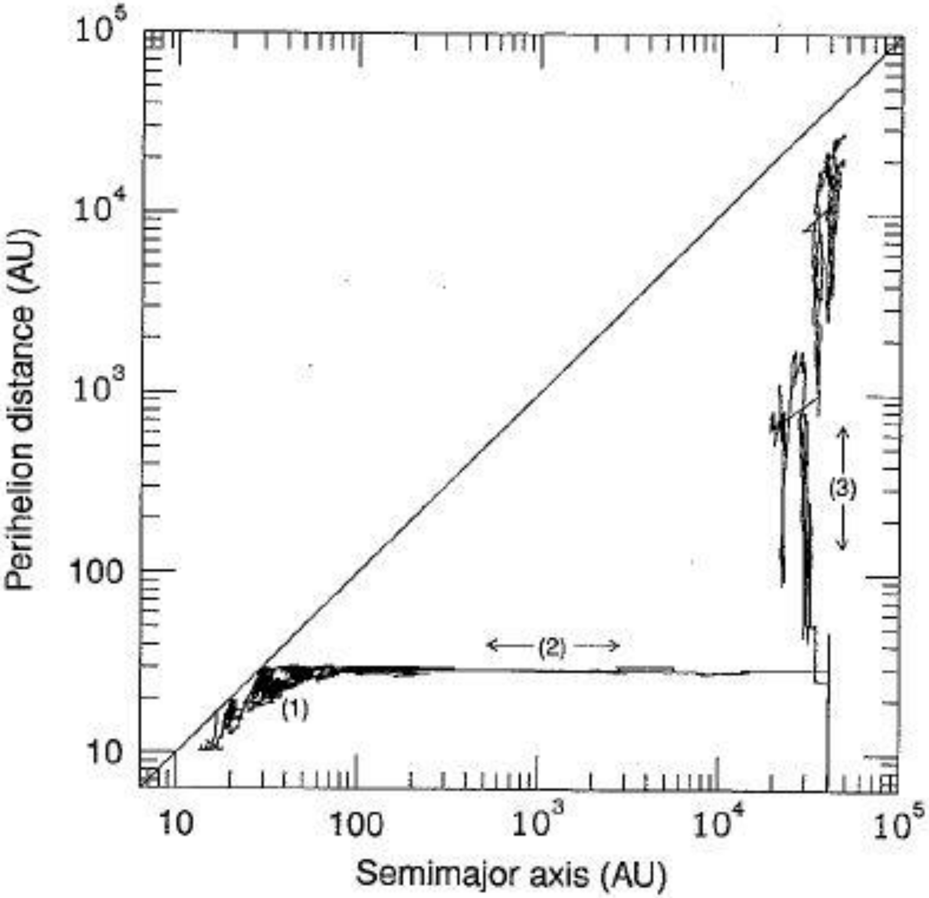

Figure 10.40 The dynamical evolution of an object as it evolves into the Oort cloud. The object began on a nearly circular orbit between the giant planets. In the initial phase of the evolution (1), the object remains in a moderate eccentricity orbit in the giant planet region. Neptune eventually scatters it outward, after which it undergoes a random walk in inverse semimajor axis (2). When the orbit becomes almost parabolic, the galactic tidal force can raise its perihelion above the planetary region (3). (Levison and Dones 2007)

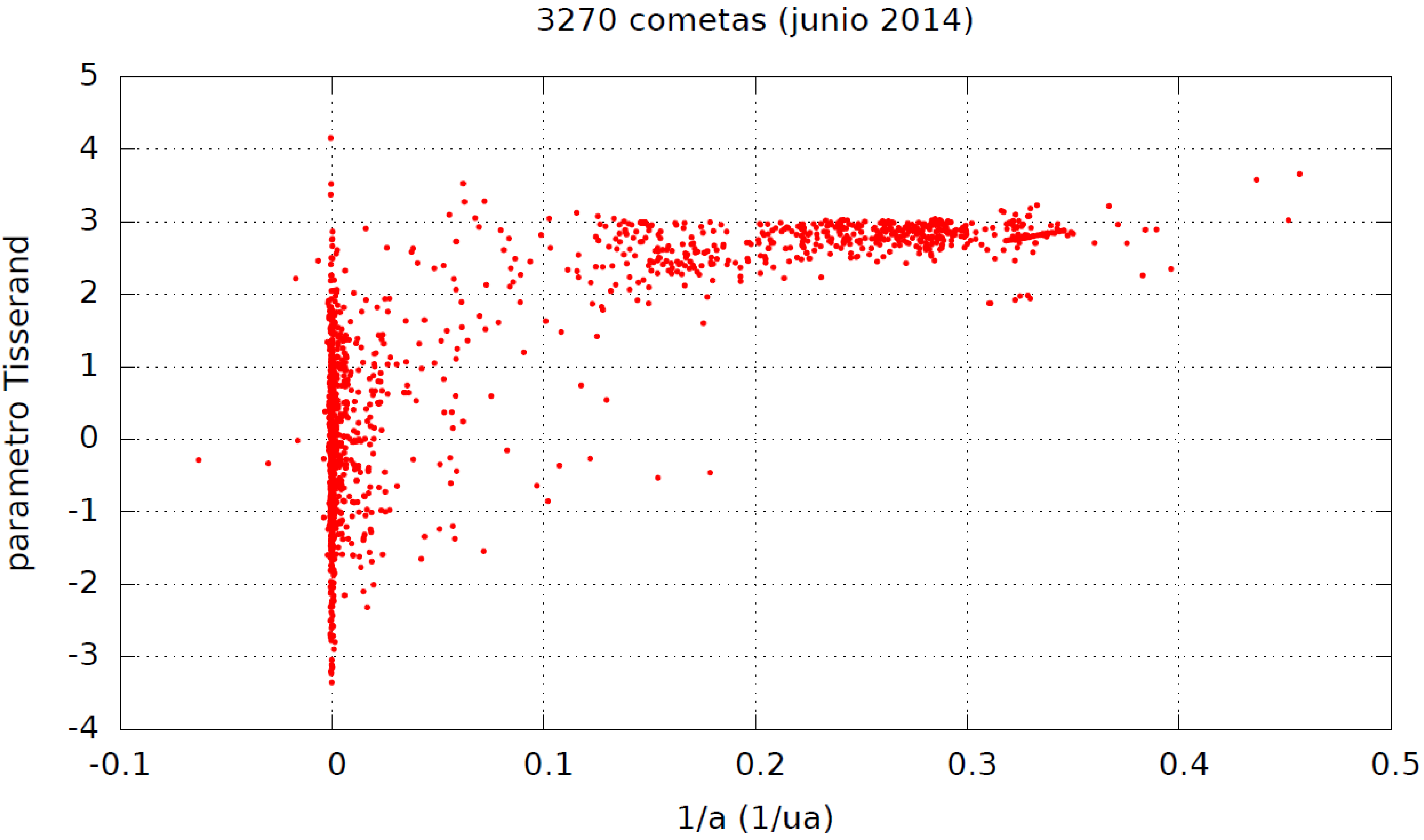
3270 cometas (junio 2014)
parametro Tisserand
5
4
3
2
1
0
-1
-2
-3
-4
-0.1
0
0.1
0.2
0.3
0.4
0.5
1/a (1/ua)

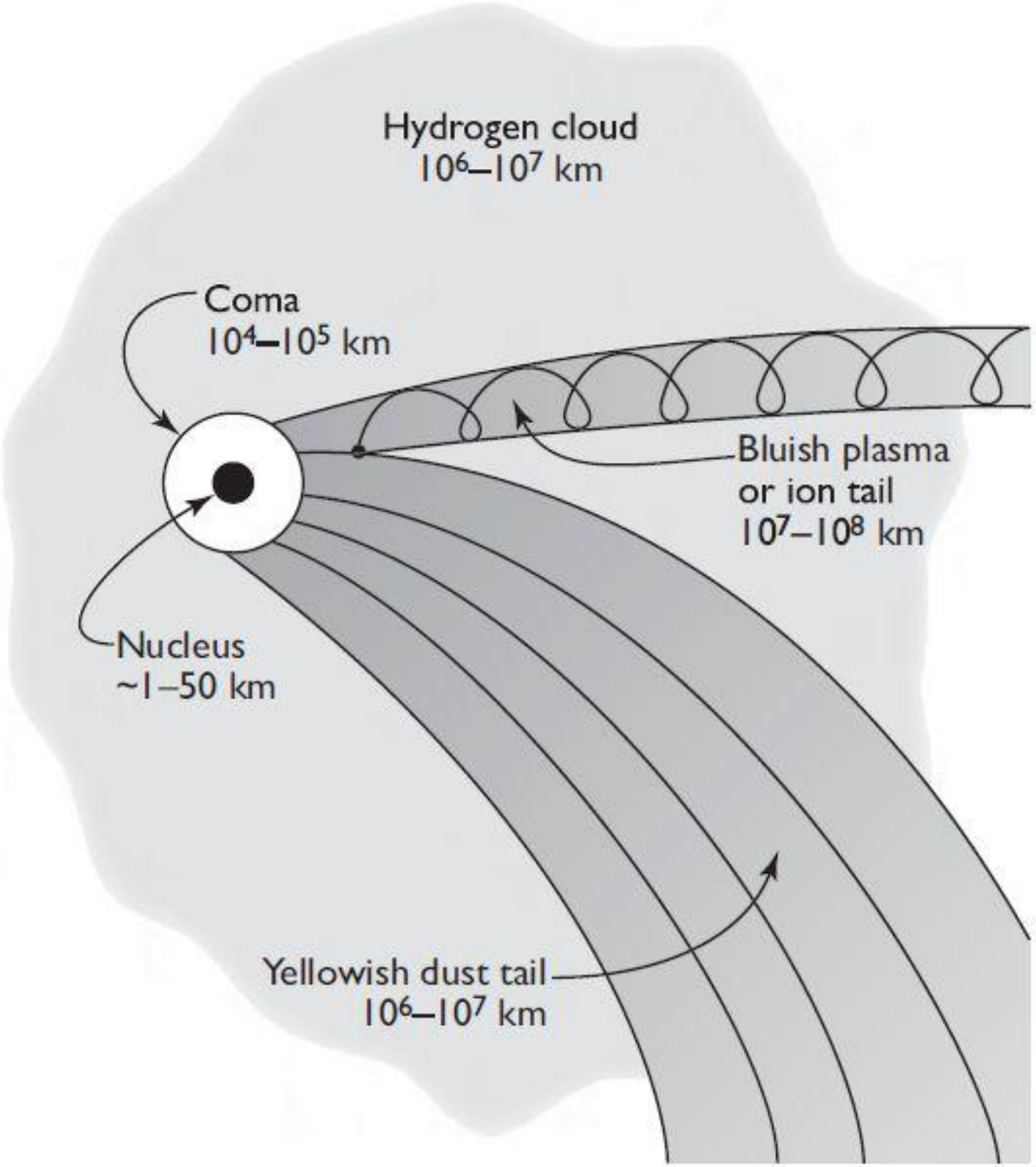

Figure 12.28 Schematic diagram of a comet, showing its nucleus, coma, tails and hydrogen cloud. (de Pater and Lissauer, 2010)

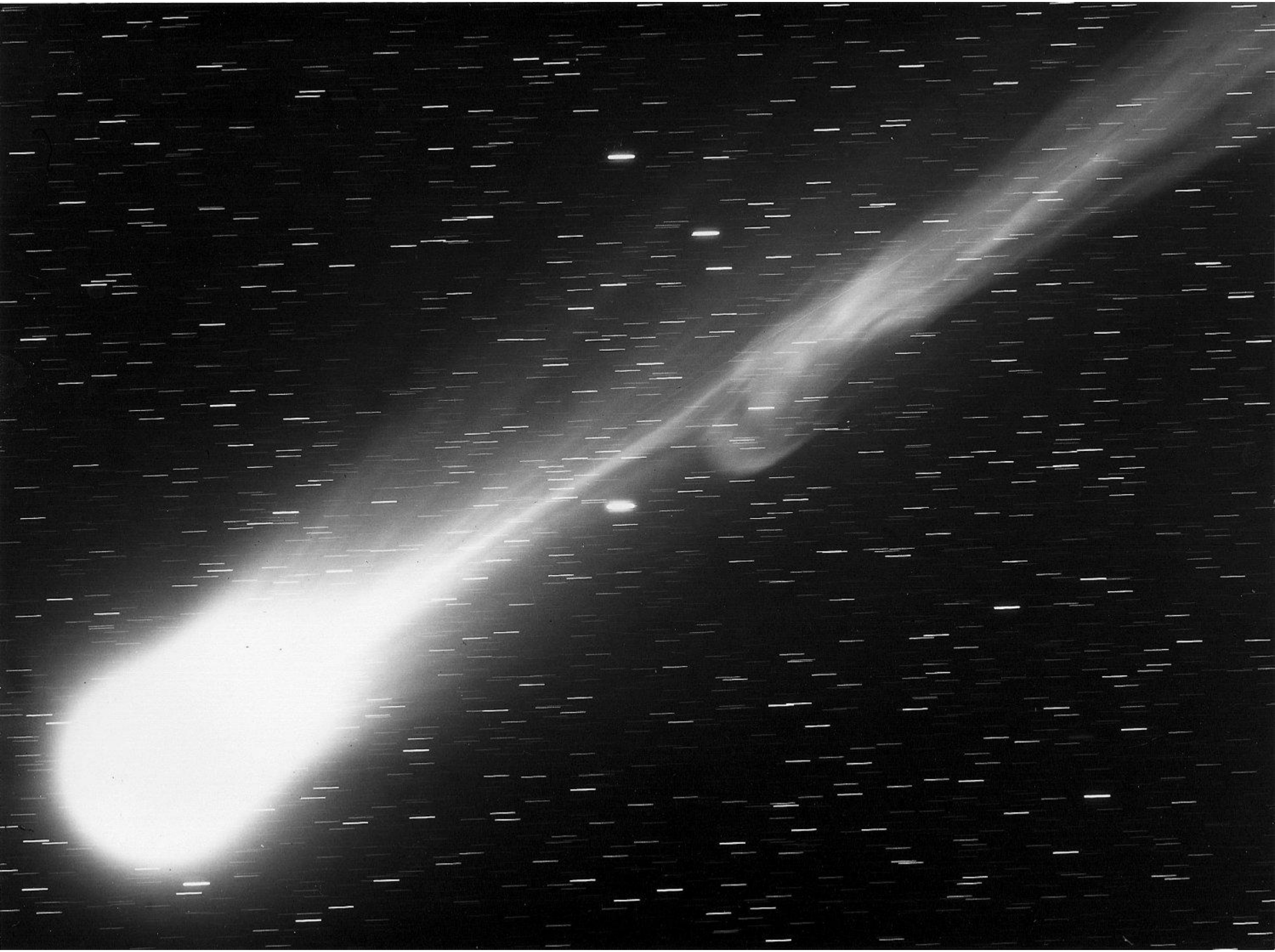

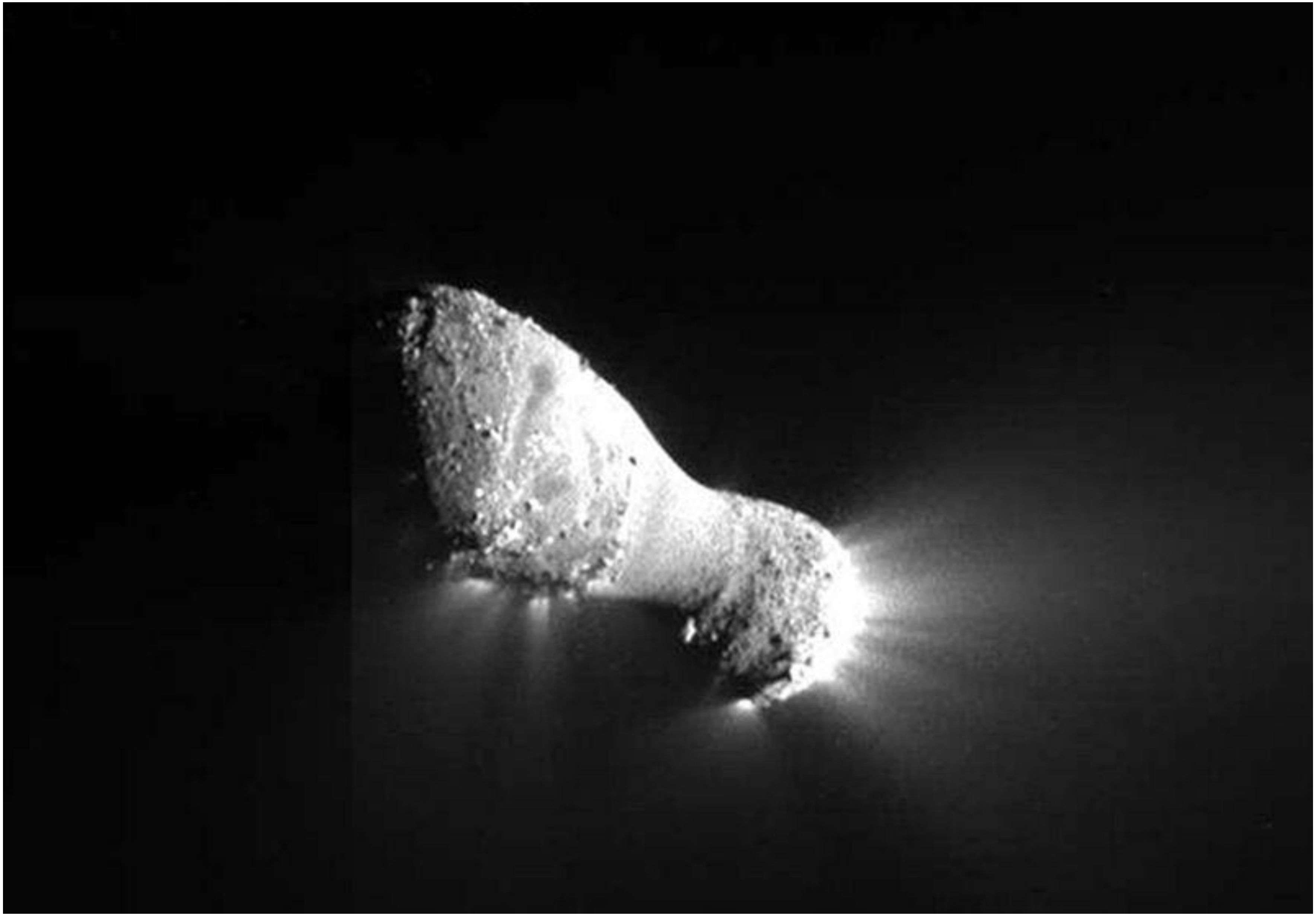

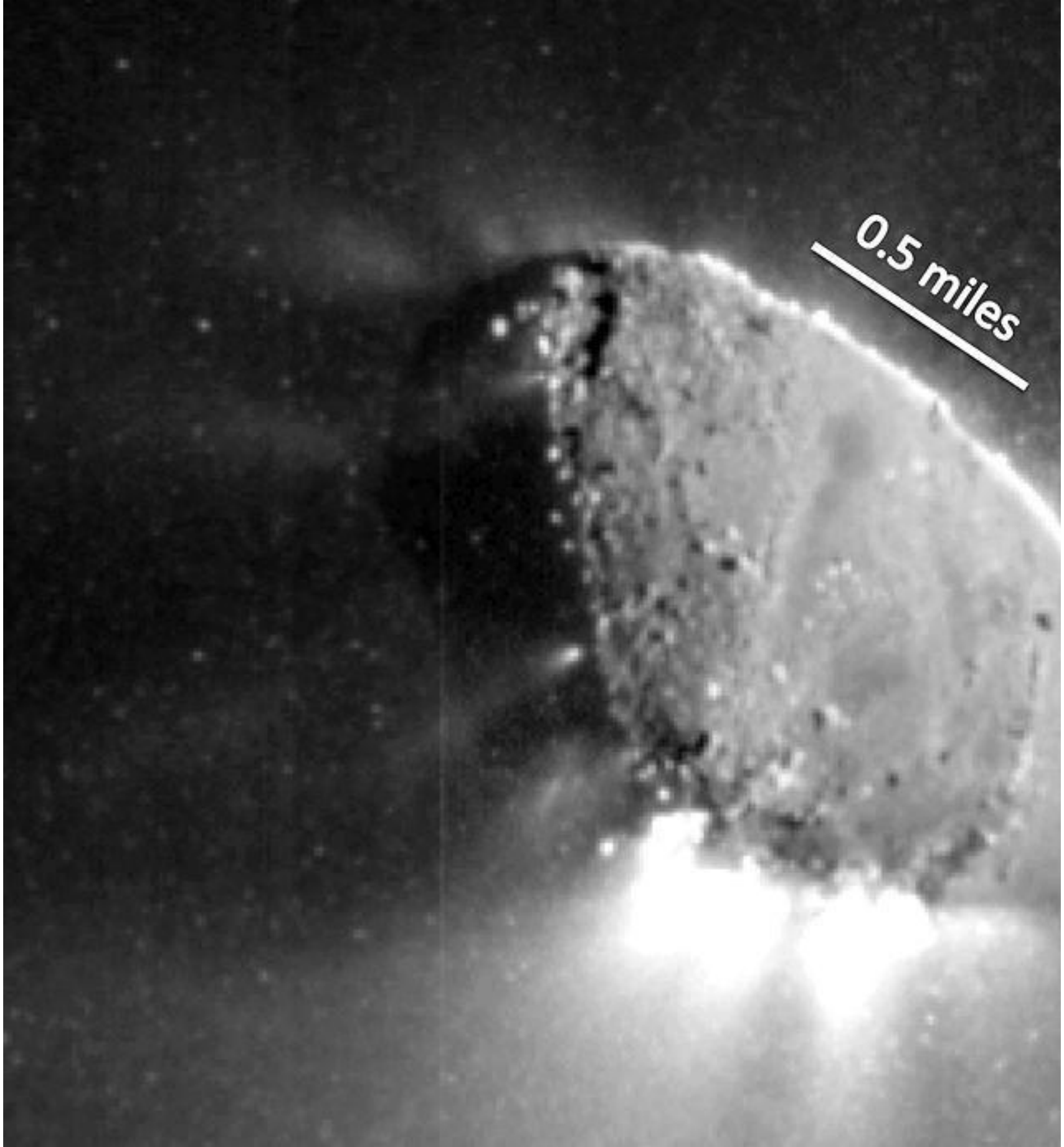
0.5 miles

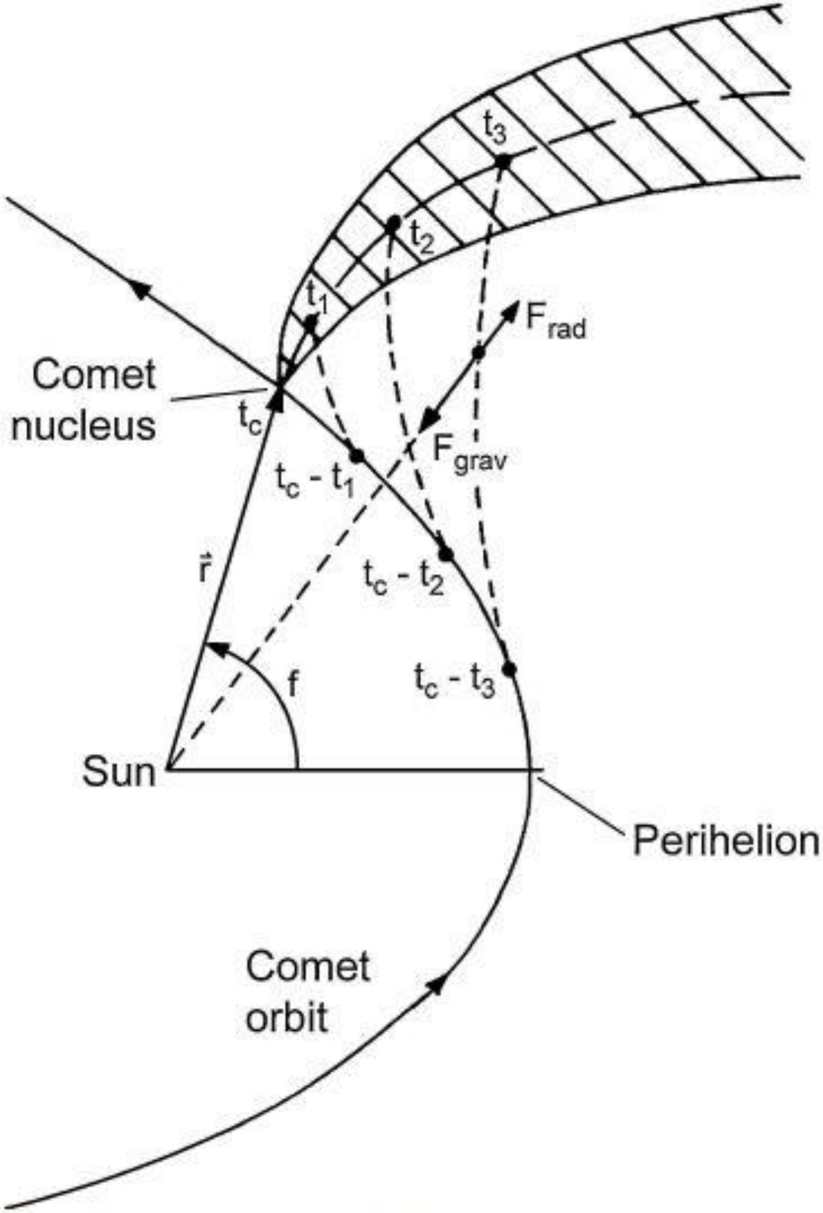

Figure 3.16. The differential motion of the dust particles with respect to the comet nucleus, under the action of the radiation pressure, generates de dust tail.

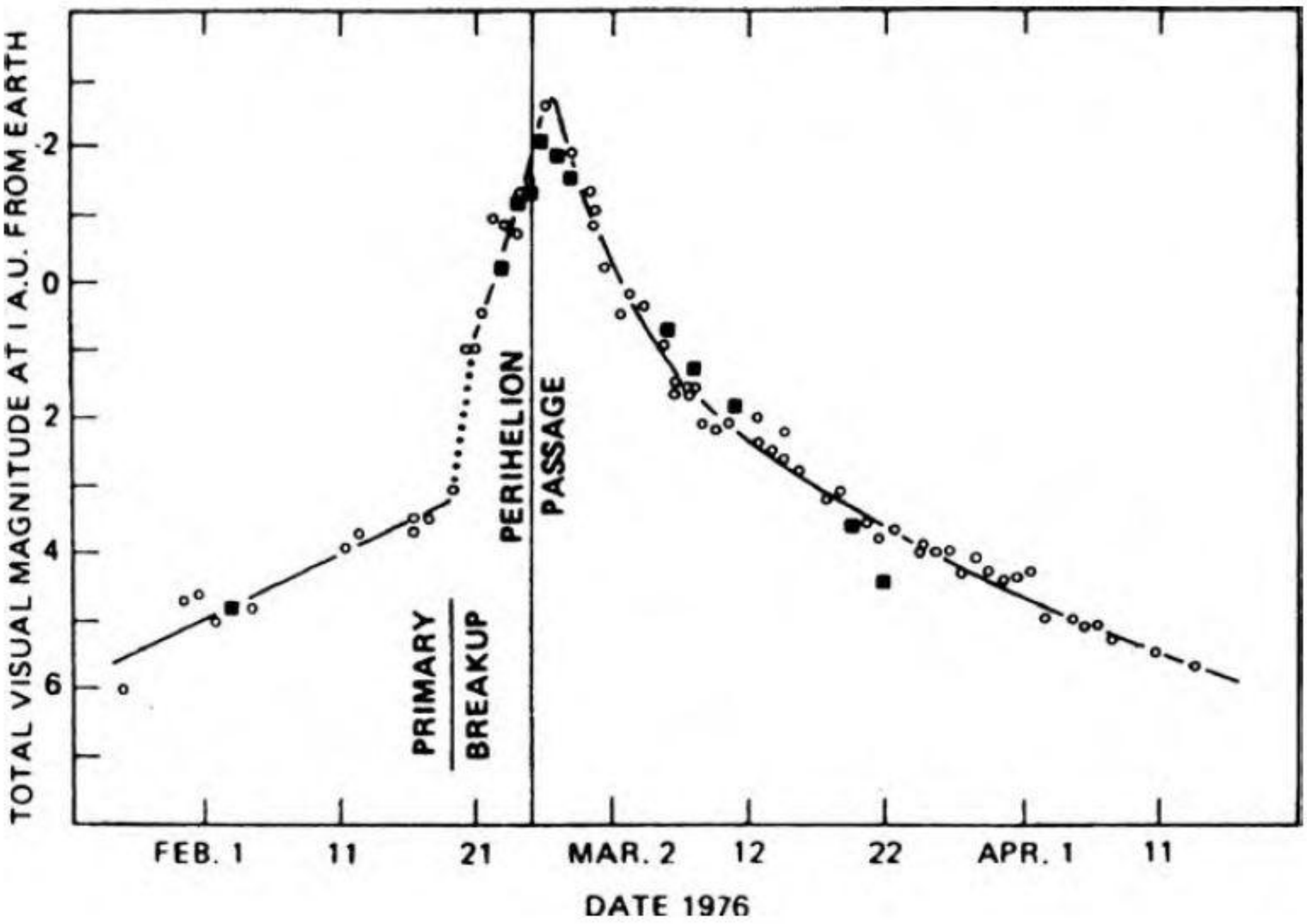

Figure 12.13 The lightcurve of C/West, which shows evidence of a splitting event (indicated in the figure). (Sekanina and Farrell 1978)

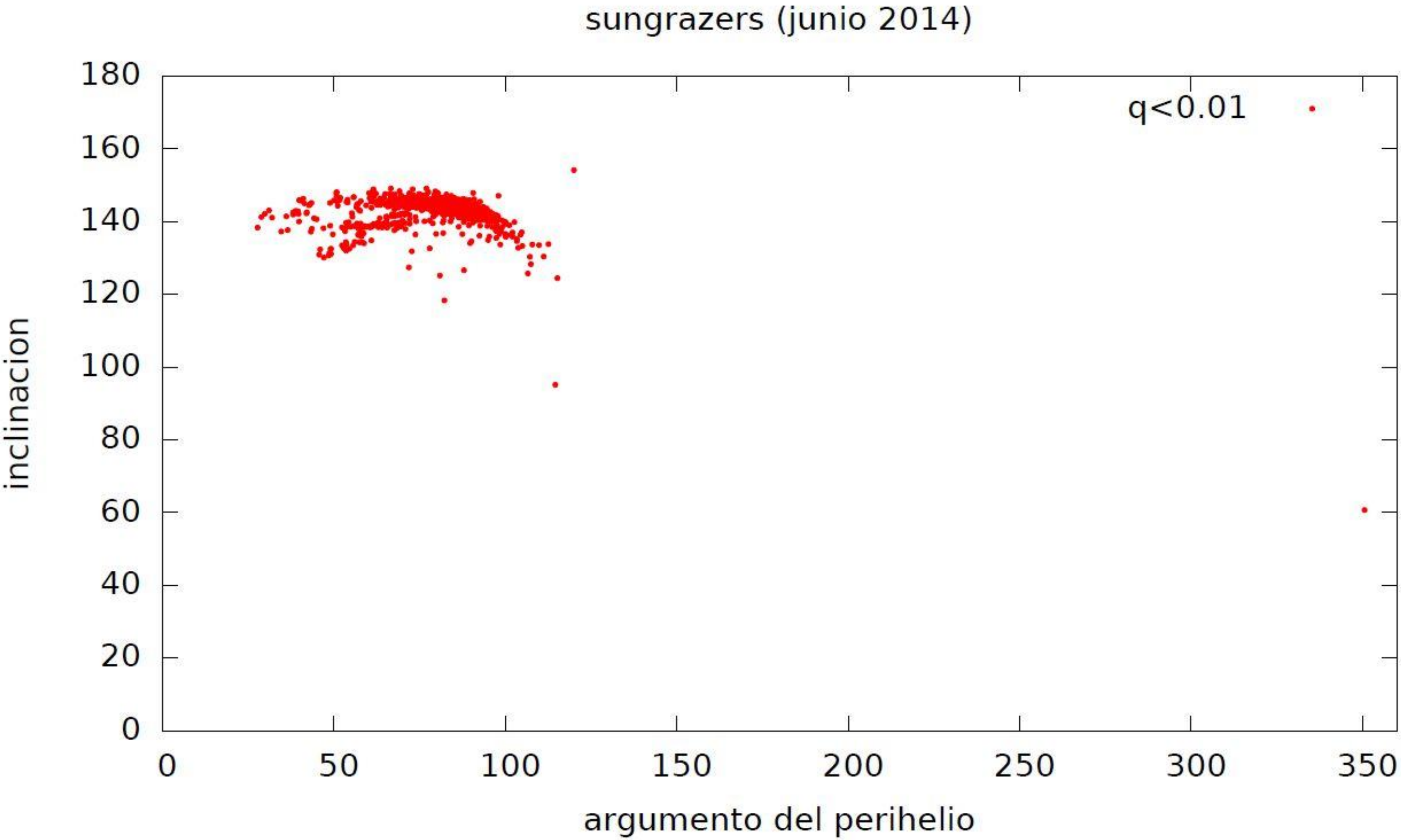
sungrazers (junio 2014)
q<0.01
inclinacion
argumento del perihelio
0
20
40
60
80
100
120
140
160
180
0
50
100
150
200
250
300
350

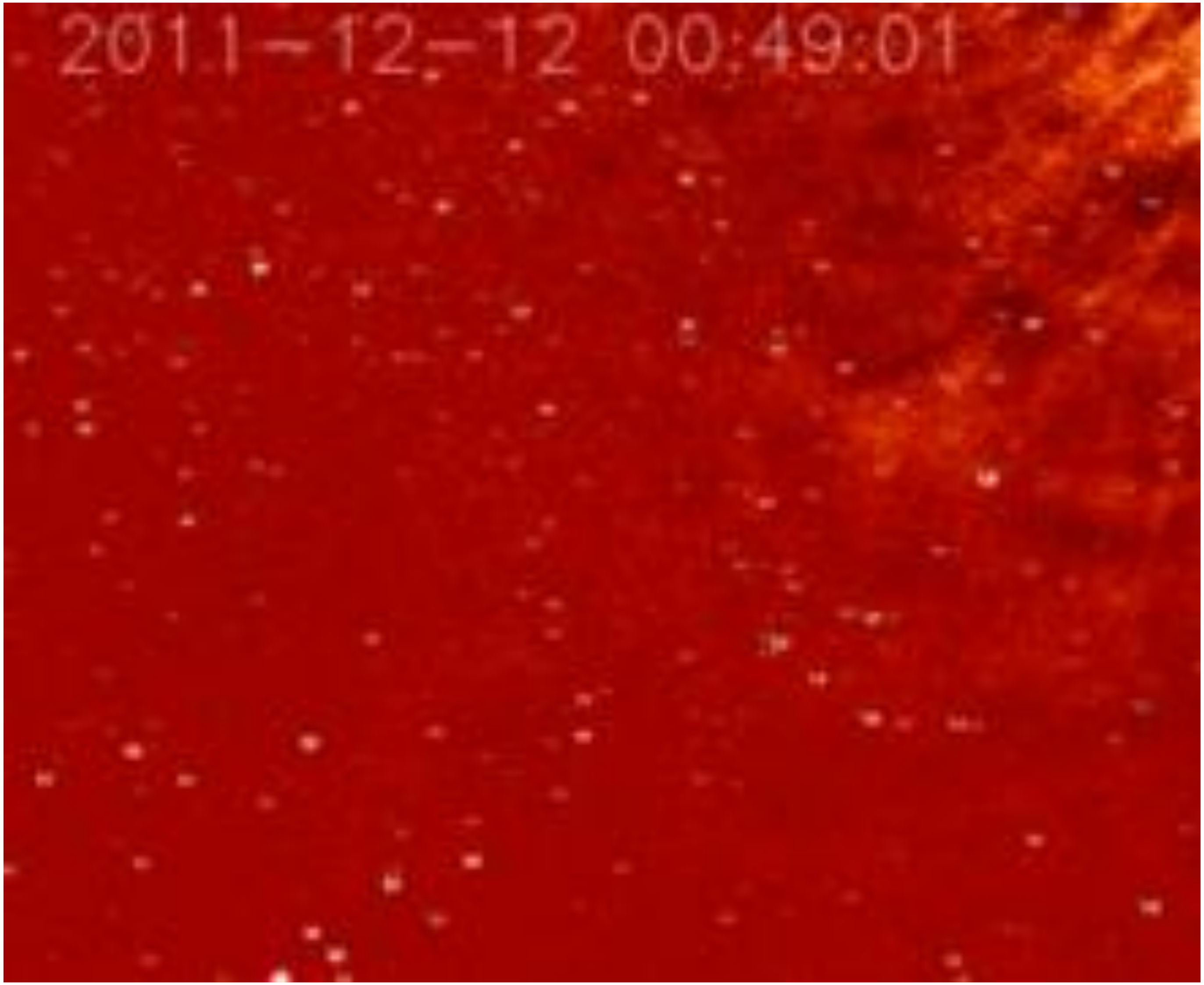
2011-12-12 00:49:01

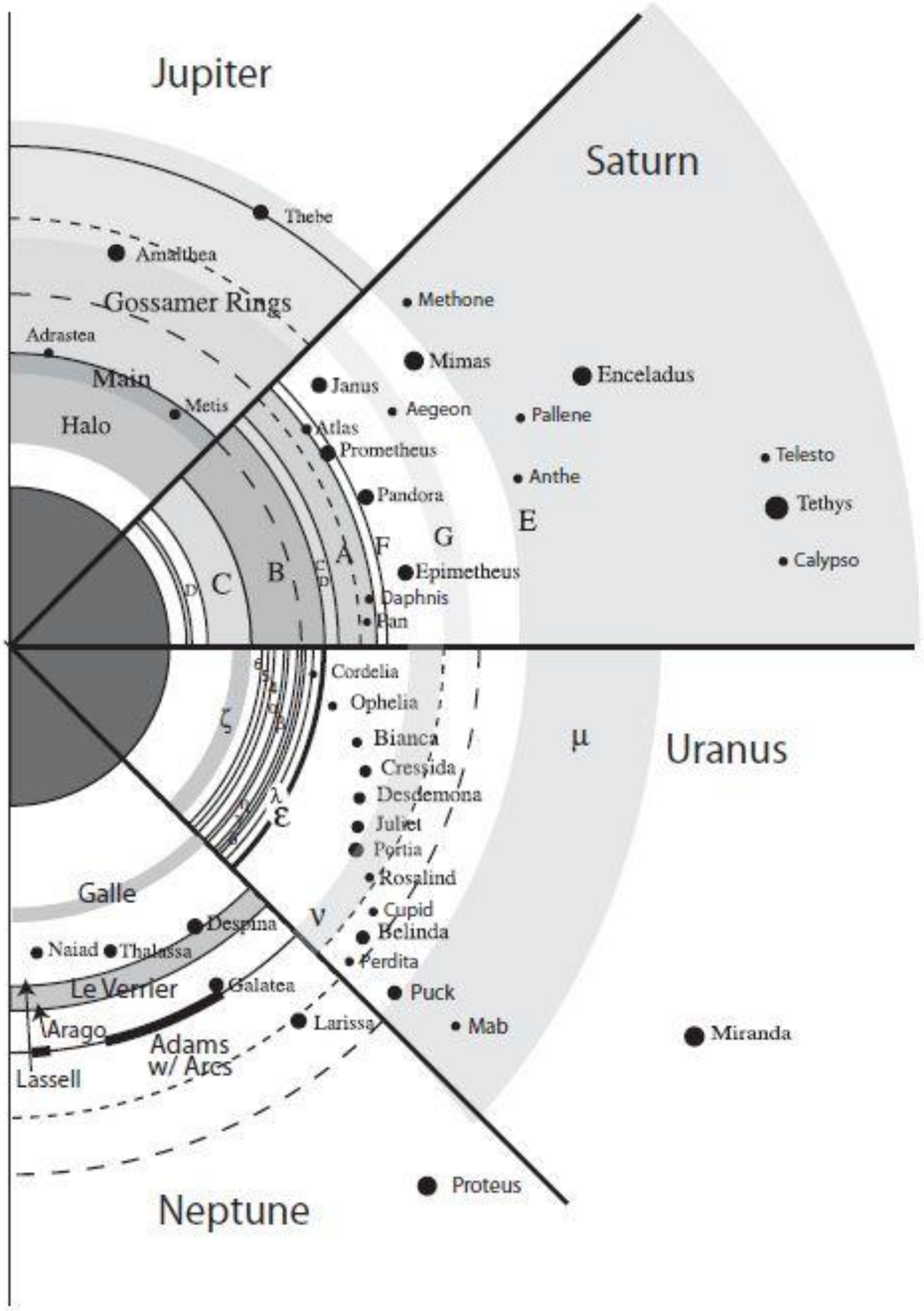
Jupiter
Saturn
Uranus
Neptune
Thebe
Amalthea
Gossamer Rings
Adrastea
Main
Metis
Halo
Methone
Mimas
Enceladus
Janus
Aegeon
Pallene
Atlas
Prometheus
Telesto
Anthe
Pandora
Tethys
E
G
F
A
B
C
D
Calypso
Epimetheus
Daphnis
Pan
Cordelia
Ophelia
ζ
Bianca
μ
Cressida
Desdemona
λ
ε
Juliet
Portia
Rosalind
Galle
Cupid
Despina
ν
Belinda
Naiad
Thalassa
Perdita
Le Verrier
Galatea
Puck
Arago
Larissa
Mab
Miranda
Adams
w/ Arcs
Lassell
Proteus

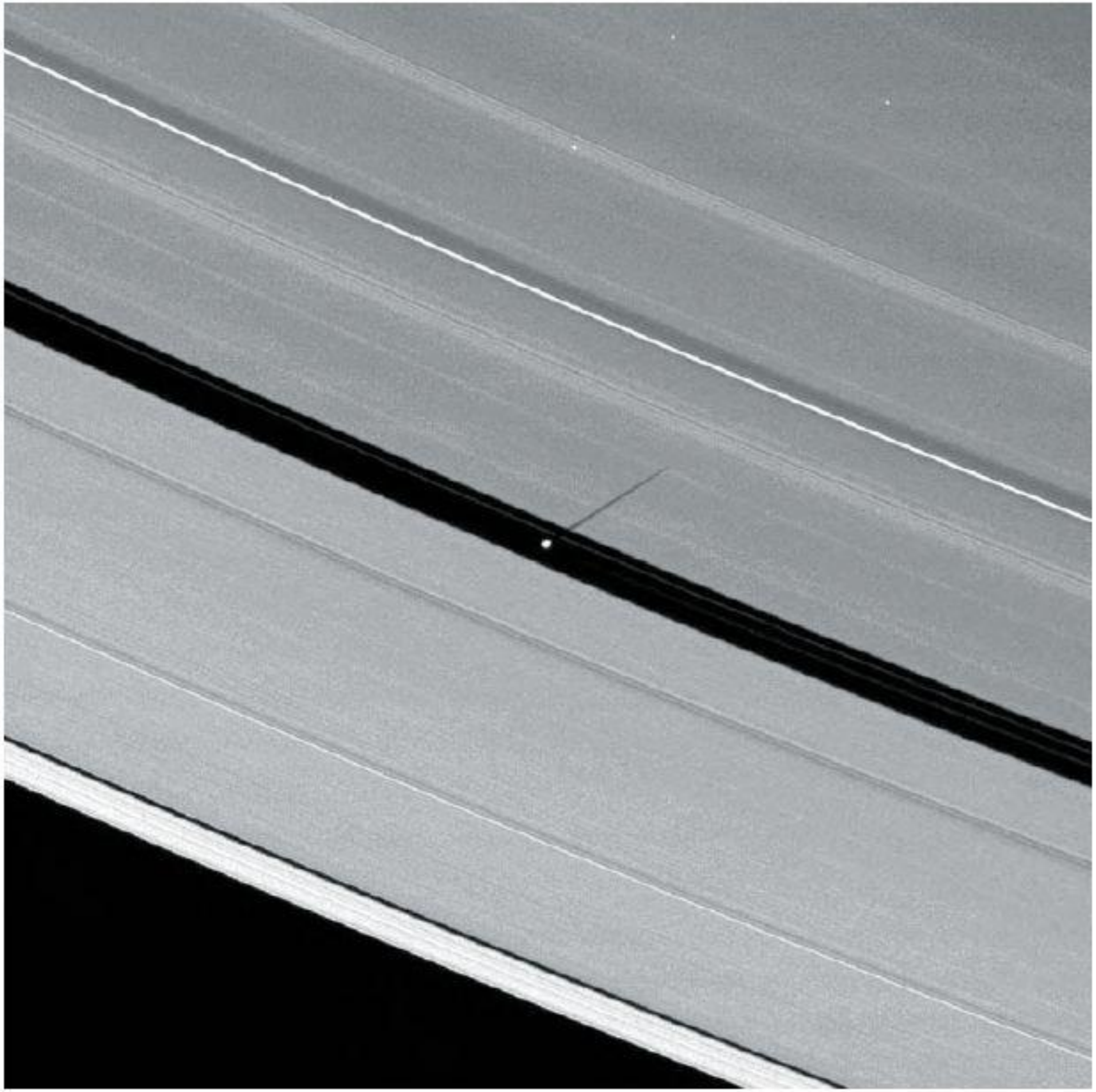

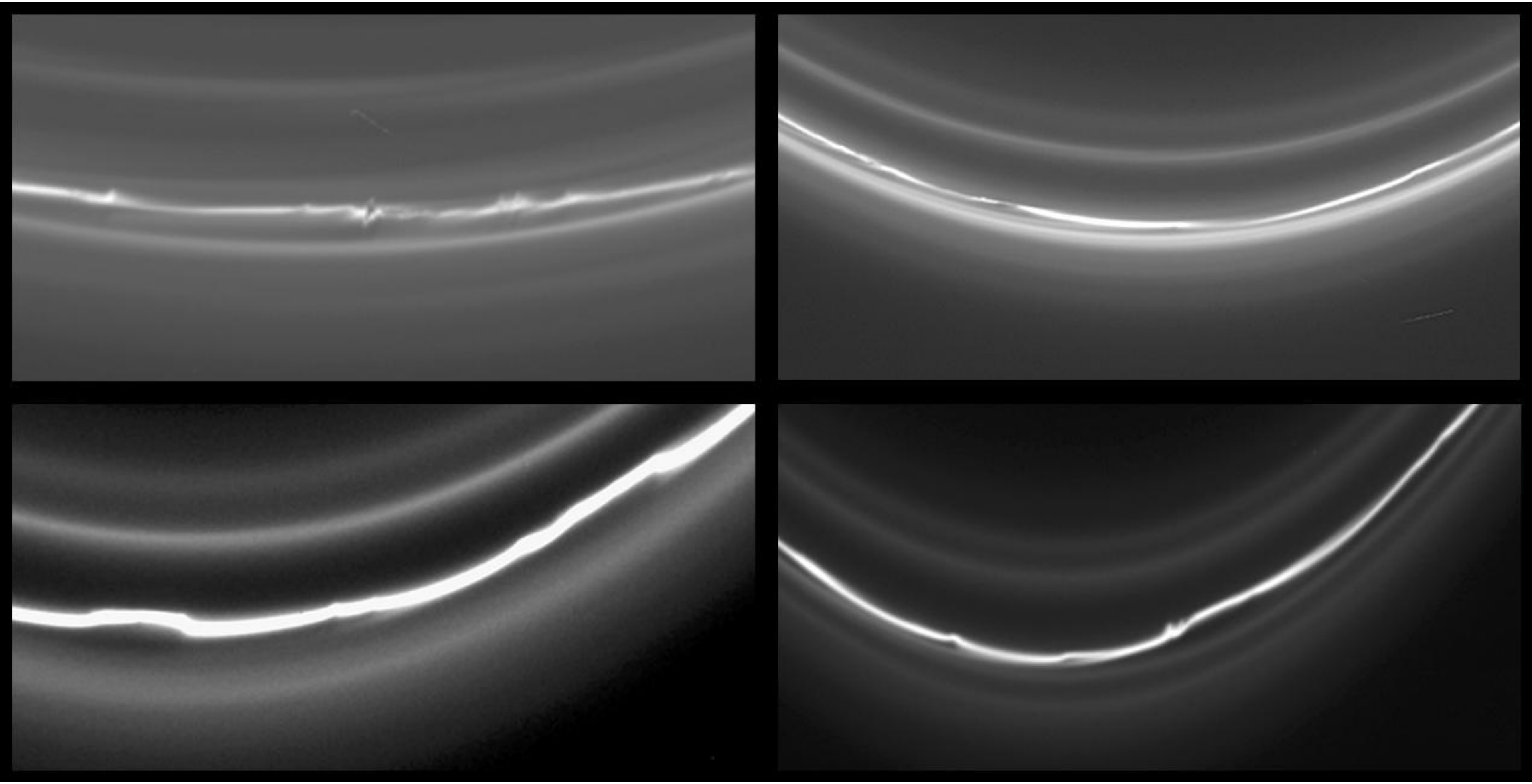

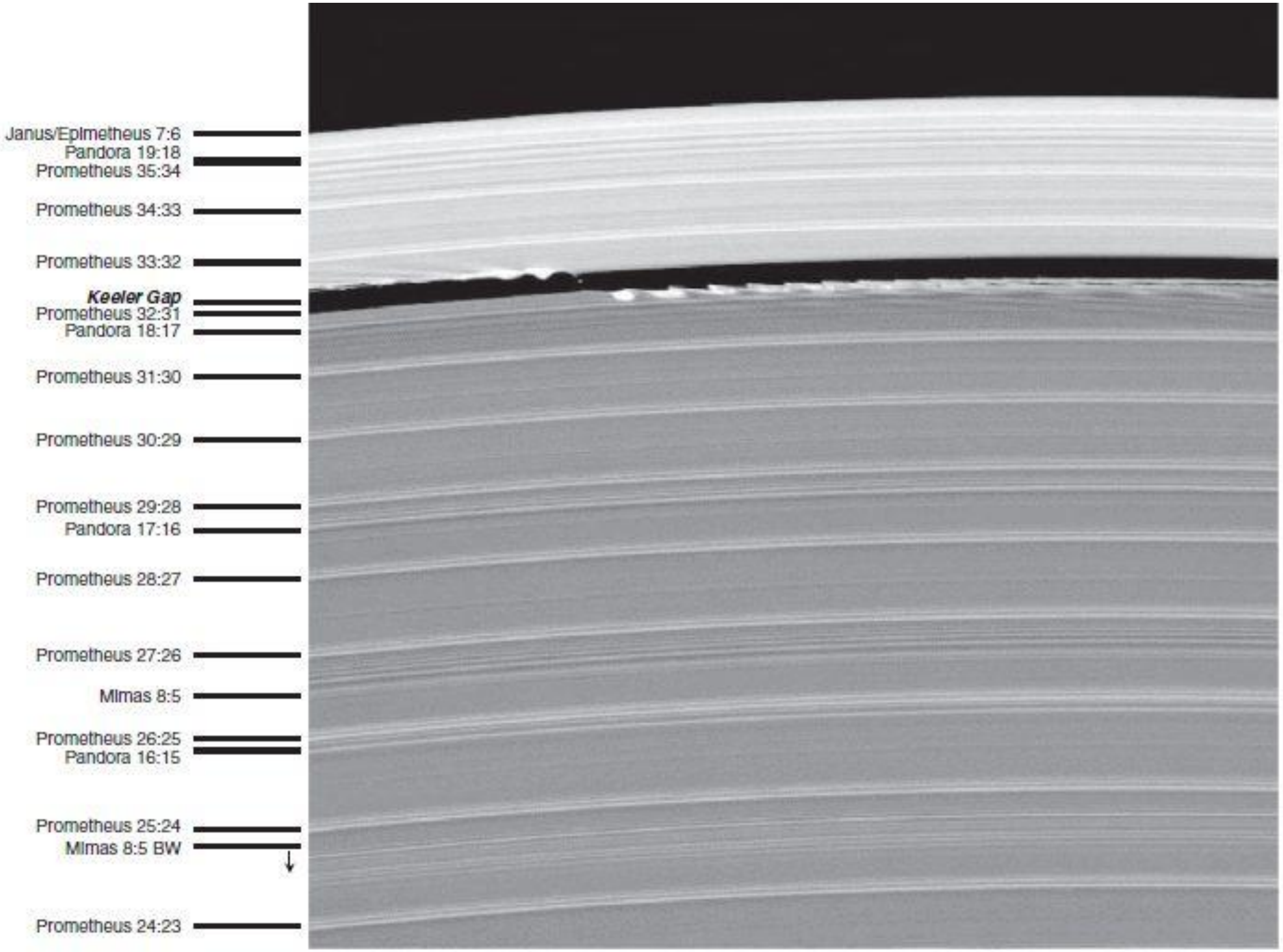

Figure 13.19 *Cassini* image of the lit face of the outer portion of Saturn's A ring, with the locations of strong satellite resonances and the Keeler gap marked on the left. The Janus/Epimetheus 7:6 ILR confines the outer edge of the A ring. The first few crests and troughs of the inwardly propagating Mimas 8:5 bending wave and the outwardly propagating Mimas 8:5 density wave can be seen on this image, whereas the wavelengths of the higher m_θ density waves at the resonances of the nearby small moons are shorter and not clearly discernible in this version. The tiny moon Daphnis is to the left of center, and its effects on the edges of the Keeler gap are quite prominent. (Image PIA07809 from NASA/JPL/CICLOPS, annotated by Matt Tiscareno)

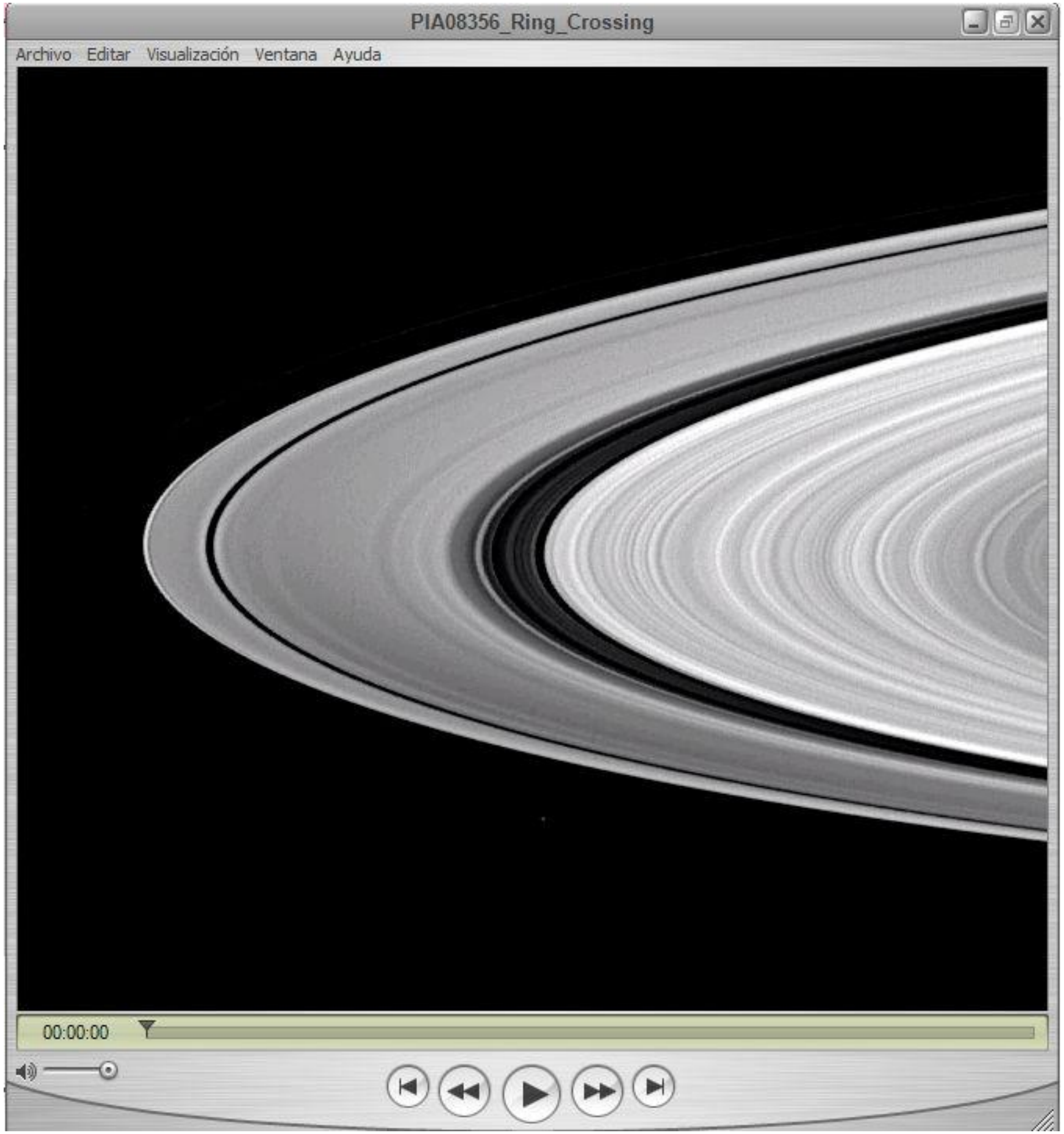
PIA08356_Ring_Crossing
Archivo
Editar
Visualización
Ventana
Ayuda
00:00:00

BIBLIOGRAFIA

Planetray Sciences
Asteroids III
www.minorplanetcenter.net
sajri.astronomy.cz/asteroidgroups/groups.htm
photojournal.jpl.nasa.gov